FRONTIERS OF PHYSICS

TOPICAL REVIEW
Volume 18 / Issue 1 / 13603 / 2023

Bifunctional oxygen electrocatalysts for rechargeable zinc–air battery based on MXene and beyond

Jing Zhang[1,2], Zixiang Cui[1,2], Jie Liu[3], Chunjie Li[2], Haoyi Tan[4,5], Guangcun Shan[4,5,†], Ruguang Ma[2,‡]

1 School of Physical Science and Technology, Suzhou University of Science and Technology, Suzhou 215009, China
2 School of Materials Science and Engineering, Suzhou University of Science and Technology, Suzhou 215009, China
3 State Key Laboratory of High-Performance Ceramics and Superfine Microstructure, Shanghai Institute of Ceramics, Chinese Academy of Sciences, Shanghai 200050, China
4 Shenzhen Beihang Emerging Industry Technology Research Institute, University Park, No. 2 Yuexing Three Road, Shenzhen 518052, China
5 School of Instrumentation Science and Opto-electronics Engineering, Beihang University, Beijing 100083, China
Corresponding authors. E-mail: †gcshan@buaa.edu.cn, ‡ruguangma@usts.edu.cn

ABSTRACT

Oxygen electrocatalysts are of great importance for the air electrode in zinc–air batteries (ZABs). Owing to large surface area, high electrical conductivity and ease of modification, two-dimensional (2D) materials have been widely studied as oxygen electrocatalysts for the rechargable ZABs. The elaborately modified 2D materials-based electrocatalysts, usually exhibit excellent performance toward the oxygen reduction reaction (ORR) and oxygen evolution reaction (OER), which have attracted extensive interests of worldwide researchers. Given the rapid development of bifunctional electrocatalysts toward ORR and OER, the latest progress of non-noble electrocatalysts based on layered double hydroxides (LDHs), graphene, and MXenes are intensively reviewed. The discussion ranges from fundamental structure, synthesis, electrocatalytic performance of these catalysts, as well as their applications in the rechargeable ZABs. Finally, the challenges and outlook are provided for further advancing the commercialization of rechargeable ZABs.

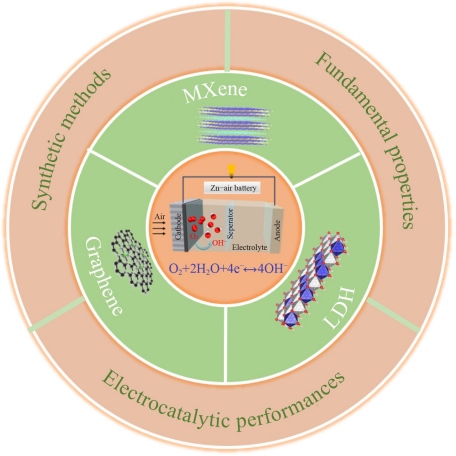

Keywords MXenes, oxygen reduction reaction, oxygen evolution reaction, electrocatalysts, zinc–air battery

Contents

* Special Topic: MXene and Its Applications (Eds.: Qing Huang, Ju Han Lee & Guangcun Shan).

Higher Education Press

https://doi.org/10.1007/s11467-022-1208-8

1 Introduction

The current energy supply is hard to meet the new energy demand brought by the rapid population increase and economy development. Renewable clean energy is highly needed under the current situation of carbon neutrality [1]. Lithium-ion batteries (LIBs) provide a strong guarantee for various portable electronic devices as well as most of electric vehicles [2–4]. Although LIBs have achieved significant success in business, there are still some insurmountable problems in the practical applications [5–9]. For example, high manufacturing cost and low energy density are obviously unable to satisfy the requirement of long-term lifetime and long-range transport. More importantly, LIBs themselves possess safety risks at some special situations, such as short circuit [10–12]. As a result, researchers have begun to look for alternatives.

As potential alternatives, batteries based on aqueous electrolyte have gradually attracted researcher's attention among different battery systems. Zinc–air batteries (ZABs) are a kind of promising candidate owing to their attractive features, such as large theoretical energy density, low manufacturing cost and inherent safety [13–16]. What's more, there is no hazardous electrolyte in the ZABs, which avoids the potential puzzle for recycle [17, 18]. However, due to the inherently slow kinetics of the oxygen reduction reaction (ORR) and oxygen evolution reaction (OER) [19, 20], the unsatisfactory performance and short life have become the primary limitations of commercial applications. Therefore, based on the significant advantages of resource and cost of Zn, it is necessary to explore the efficient and durable bifunction electrocatalysts to boost the reaction kinetics of ORR and OER [21]. ZABs would be an economically viable solution to alleviate the energy crisis and environmental pollution.

During the discharge/charge process (ORR/OER), the reaction kinetics at the air electrode is much slower compared to that at the Zn electrode [22], and the overpotential is greater at the same current density. Therefore, highly efficient electrocatalysts are required during the charge/discharge process to reduce the energy barrier of OER/ORR and to promote the efficient reaction rate. At present, the commonly used catalyst for ORR and OER is commercial Pt/C [23], and commercial RuO_2 [24], respectively. Due to the scarcity of noble metal resources, the electrocatalysts based on noble metal are expensive, which seriously restricts the development of ZABs. At the same time, precious metal nanoparticles are mainly supported by carbon particles (Pt/C and Ir/C), which is not conducive to the long-term operation of ZABs to some extent, because there will be a risk of nanoparticle agglomeration in the concentrated alkaline solutions. Among many alternative materials, two-dimensional (2D) materials have become a promising candidate as electrocatalysts themselves or supports of electrocatalysts, due to their intrinsic advantages such as large specific surface area, abundant functional groups at the surface, and adjustable band gap [25]. Moreover, the ideal layer structure provides a good platform for theoretically studying their fundamental properties and structure-performance relationships during the ORR/OER process [26].

Recently, with the advancement of materials science and nanotechnology [27–30], ZABs have attracted the new interests of researchers. In the past decade, significant progress and exciting breakthroughs have been made in anode structure, electrolytes, and electrocatalysts, which have greatly promoted the commercialization of ZABs [31–35]. Given the recently rapid development in ZABs, there have been many reviews on the design and preparation of ZABs, such as quasi-solid-state batteries, neutral electrolytes, and hybrid zinc systems. Herein, the electrocatalysts based on typical two-dimensional (2D) materials, such as MXenes, graphene and layered double hydroxides (LDHs) are systematically summarized, with particular attention to the research articles published in the past three years. The latest advances on these high-performance electrocatalytic materials will be discussed as well as the performance of ZABs. In addition, the current challenges will also be discussed. Finally, we will propose potential avenues for further research on ZABs to shorten the road to commercialization.

2 Zinc–air batteries

Zinc-air batteries typically consist of air cathode, zinc anode, electrolyte and separator as shown in Fig. 1. The first zinc-air battery has been introduced to the market as a power source for hearing aids and pagers as early as the 19th century, which is a primary battery with the

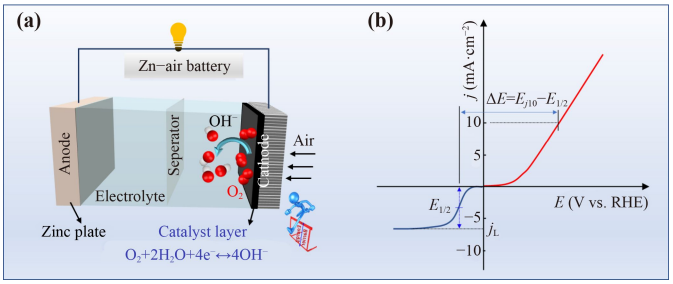

Fig. 1 **(a)** Schematic illustration of zinc–air battery and **(b)** the key parameters indicating the electrocatalytic activity of bifunctional oxygen electrocatalysts.

actual energy density from 200 to 500 $Wh \cdot kg^{-1}$ [36]. For rechargeable ZABs, the reaction at the air electrode is: $O_2 + 2H_2O + 4e^- \leftrightarrow 4OH^-$ under alkaline conditions. During the discharge process, oxygen diffuses into the air electrode layer and is reduced to hydroxyl ions under the action of an active electrocatalyst. Hydroxyl ions are transferred to the zinc anode through a separator and then bond with zinc ions to form soluble zincate ions, which decompose into ZnO when the ions reach saturation in the electrolyte. During the process, electrons released by the zinc reaction with a hydroxyl group are transferred to the air cathode [37]. During the charge process, the OER process is accelerated at the air electrode by an electrocatalyst, while the ZnO decomposes into Zn and O_2. The specific reactions are shown as below:

$$\text{Air cathode}: O_2 + 2H_2O + 4e^- \rightarrow 4OH^-,$$

$$\text{Zinc anode}: Zn \rightarrow Zn^{2+} + 2e^-,$$

$$Zn^{2+} + 2OH^- \rightarrow Zn(OH)_2,$$

$$Zn(OH)_2 \rightarrow ZnO + H_2O,$$

$$\text{Total reaction}: 2Zn + O_2 \rightarrow 2ZnO.$$

The ORR (discharge) process and OER (charge) process at the cathode of rechargeable ZABs include a series of complex electron transfer reactions, involving four electron reaction steps. Generally, the ORR proceeds through the formation of *OOH from adsorbed O_2, followed by the further reduction to *O and *OH (* refers to active sites on the catalyst) [38]. The OER takes place just in the opposite sequence. Before and after an electron transfer, the largest difference of binding energy of different intermediates (i.e., *OH, *O, and *OOH) results in an overpotential. The overpotential during the ORR/OER at the air electrode, causes a low round-trip energy efficiency of rechargeable ZABs below 55%–65% [39]. The main obstacle to achieve bifunctional catalytic activity towards the OER and ORR in one material lies in the interdependence of the adsorption energies towards OH groups and O_2 molecules. Therefore, it is necessary to achieve a good balance between the formation energies of *OH and *OOH intermediates via the design of material structure, composition, and electronic states.

The performance of electrocatalysts in the air electrode directly affects the performance of ZABs, including power density, energy efficiency, and cycle life. The design of air electrodes usually by coating a suitable catalyst on a gas diffusion layer (GDL) treated with polytetrafluoroethylene (PTFE) [40, 41]. The inexhaustible oxygen in the air ensures the reaction of the air electrode. Since the efficiency of rechargeable ZABs is dominantly determined by the electrocatalyst, a reasonable evaluation method is established to evaluate the performance of electrocatalysts, prior to the entire battery. For ORR catalysts, the performance of electrocatalysts is usually evaluated by comparing the reduction peak potential, the onset potential, the half-wave potential ($E_{1/2}$), and the diffusion-limiting current density (j_L) as shown by the left panel in Fig. 1(b), while the stability also needs to be considered. When evaluating the performance of the OER catalyst, the most common strategy is to estimate the overpotential to achieve a current density of 10 $mA \cdot cm^{-2}$ (E_{j10}) as shown by the right panel in Fig. 1(b) [42]. The electrocatalytic activity of bifunctional electrocatalyst toward ORR and OER is usually evaluated by the difference of potential between E_{j10} for OER and $E_{1/2}$ for ORR ($\Delta E = E_{j10} - E_{1/2}$) as marked in Fig. 1(b). Platinum and its alloys have been considered as the benchmark material for ORR [43], and RuO_2 or IrO_2 for OER [44]. Despite the excellent properties as catalysts, the high cost and poor reserves limit their large-scale applications. The catalyst based on noble metal has excellent performance for OER, which is difficult to achieve an excellent performance for ORR, vice versa. It is difficult to achieve a balance of good OER and ORR activity at the same time. The OER process requires a large potential (1.6 V vs. RHE or even higher) [39], which means that the ORR catalyst is inactivated during charging. In this sense, the development of electrocatalysts with high performance plays a crucial role in the process of reducing the overpotential and excitation of OER. Therefore, the design and preparation of low-cost electrocatalysts with both excellent OER and ORR performance is of great significance for the commercialization of ZABs.

For zinc–air batteries, the choice of electrolyte also has a significant impact on the performance of the battery, such as overall stability of electrochemistry, voltage window and even reaction mechanism. The electrolyte provides the basic operating environment for the ZABs, ensuring a high degree of compatibility and reversible operation of the battery. In addition, these by-products are loosely stacked on the surface and make damage for the cycle performance of the ZABs. When zinc is nucleated in the substrate, the absorbed Zn^{2+} ions will diffuse laterally, which will lead to the formation of protruding tips at the location of charge transfer. What's more, the tips will continuously attract more Zn ions that cause the accumulation and overlap, eventually forming zinc dendrites [45, 46]. The separator also greatly affects the chemical stability and working life. The excellent mechanical strength can ensure the separator not to be punctured by dendrites and avoid the short circuit. At the same time, the separator with high porosity has excellent ionic conductivity to ensure the free passage of electrolyte ions. The most common separators in ZABs are glass fiber, polypropylene, and PDMS-PEO. Glass fiber separators are composed of overlapping fibers with a porous structure and a large aperture. Polypropylene diaphragms have a small pore size (average 64 nm) and PDMS-PEO has higher ionic conductivity [47].

3 Two-dimensional electrocatalysts

Two-dimensional (2D) materials hold the unique properties such as large specific surface area, good electrical conductivity and abundant surface functional groups, which provide a good platform for the modification of electrocatalysts. For example, large specific surface area would provide much more active sites for the electrocatalysis. And good electrical conductivity is a prerequisite to the electrode materials. Functional groups at the surface make it possible to adjust the adsorption/desorption of reactants or reaction intermediates. Therefore, to develop high-efficient bifunctional electrocatalysts, it is necessary to summarize and analyze the latest progress of typical 2D materials-based electrocatalysts used in rechargeable ZABs in the recent years.

3.1 MXenes

Metal carbides/nitrides (MXenes) have received extensive attention in the field of electrocatalytic materials due to their excellent properties [48]. The generation of early TM carbides/nitrides is mainly achieved by etching elements in the ternary MAX phase ($M_{n+1}AX_n$) as shown in Fig. 2, where M represents early transition metals (Si, Ti, Sr, V, Zr, etc.), A is a Group IIIA or IVA specy, X is carbon/nitrogen, and n is an integer between 1 and 4 [49]. Compared to the strong M–X bonds, the interlayer M–A bonds and interatomic A–A bonds are much weaker, resulting in easy removal of the A atomic layers and an energetically unstable structure. Therefore, the surface terminal groups (e.g., –F, –OH, –O) are introduced during the etching process and the $M_{n+1}AX_n$-derived $M_{n+1}X_n$ MXene is usually labeled $M_{n+1}X_nT_x$, where T_x stands for the surface terminations [50]. In the

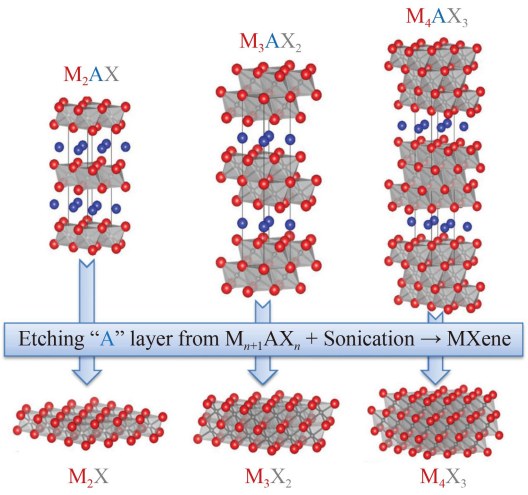

Fig. 2 Structure of MAX phases and the corresponding MXenes. Reprinted with permission from Ref. [49], Copyright © 2013 WILEY-VCH Verlag GmbH & Co. KGaA, Weinheim.

field of energy storage, 2D TM carbides/nitrides have amazing electrical conductivity, abundant surface functional groups and excellent dispersion properties in different solvents, making them hopeful for the energy storage and conversion applications. Simultaneously, MXenes have extremely rich crystal structures and surface chemistry. Moreover, the physicochemical properties of MXenes can be changed by simply modifying some functional groups to construct catalytic materials with ideal electrochemical activity.

However, the MXenes nanosheets are stacked together under van der Waals interactions, which also leads to the problem of limited active sites and slow ion motion. Researchers have tried to solve these problems by constructing 3D frameworks from 2D MXenes in recent years [51]. The 3D structures retain the large specific surface area of 2D MXene nanosheets, which is beneficial for the exposure of more active sites. The enlarged channels facilitate the rapid diffusion of electrolytes, while the abundant functional groups can serve as attractive sites for adsorption of various organic or inorganic species. Therefore, in practical applications, electrocatalytic materials based on 3D MXenes have great prospects for high-performance energy storage and conversion.

3.1.1 Synthesis

Generally, MXenes are prepared by the selective etching of "A" layers from their corresponding MAX phases by using aqueous HF as the etchant at room temperature. Upon the treatment, solid dense MAX particles are converted to a loosely packed accordion-like structure with some surface-terminating functional groups (OH, F, O, H, etc.). The etching conditions, such as etching times and HF concentrations, are important for the yields and conversion of MAX into MXene. In addition, mild etchants (e.g., NH_4HF_2) and other solvents have been also proposed to etch or exfoliate the MAX [52, 53]. Besides, the top-down etching methods, bottom-up synthesis has been also reported by Ren's group [54]. They developed a chemical vapor deposition (CVD) process, with CH_4 as the C source and a Cu foil sitting on a Mo foil as the substrate at a temperature above 1085 °C. Such high temperature makes the Cu melt and form a Mo–Cu alloy at the interface between liquid Cu and solid Mo. Subsequently, Mo atoms diffuse from the interface to the surface of liquid Cu and react with the C atoms from the decomposition of CH_4 to form high-quality 2D ultrathin α-Mo_2C crystals.

To increase the electrocatalytic performance of MXenes, doping and hybridization are commonly conducted during the synthesis process. It is an effective method to improve ORR performance by inserting nitrogen into TiC matrix. For example, Wang *et al.* [55] designed N-doped MXenes to enrich the active sites and improve the conductivity and wettability of the catalyst. In a

typical synthesis process [Fig. 3(a)] [55], 2 g LiF was dispersed in hydrochloric acid at room temperature and stirred continuously for ten minutes. Then, 2 g Ti_3AlC_2 powder was then slowly added to the above solution in an ice bath. The mixture was stirred magnetically at 40 °C for 48 hours until the pH of the supernatant reached about 6. The precipitate was centrifuged in N_2-saturated deionized water to be sonicated for 1 h, and then centrifuged at 3500 rpm for 1 h. The few-layer $Ti_3C_2T_x$ MXene was obtained by freezing the suspension in a refrigerator and then vacuum freeze-drying for four days. Afterwards, 0.025 g cobalt acetate tetrahydrate, 5 g urea, 0.5 g polyethylene glycol and 0.15 g boric acid were dissolved in 50 mL deionized water. The resulted BCN-CO precursor solution (solution A) was obtained after stirring at 80° C for 10 h. Then, 0.1 g ascorbic acid was dissolved in 25 mL N_2-saturated deionized water, and 0.02 g few layers of $Ti_3C_2T_x$ MXene was ultrasonically dispersed in ascorbic acid aqueous solution for 1 h to form solution B. TiCN-BCN-Co precursor solution was obtained by dropping solution A into solution B and stirred continuously for 10 minutes [Fig. 3(a)]. Finally, the Co rooted in 3D TiCN hybrid BCN nanotubes (TiCNeBCNeCo) was obtained after the calcination process. From the SEM image in Fig. 3(b), the 3D hybrid structure of TiCN sheets and BCN nanotubes (BCNNTs) are clearly observed.

In addition, in situ phase transformation strategy has also been widely used in the development of MXene composites. Monodisperse Ti_3C_2-Mxene nanosheets were prepared by LiF/HCl etching and liquid phase ultrasonic stripping, Then, Ti_3C_2 MXene nanosheets were dispersed into alkaline $Sr(OH)_2$ solution. Afterwards, $Sr(OH)_2$ and Ti_3C_2 MXene reacted in a hydrothermal reaction of 160 °C, and the Ti_3C_2@$SrTiO_3$ was finally obtained [Fig. 3(c)] [56]. TEM image in Fig. 3(d) clearly shows that perovskite $SrTiO_3$ nanocubes with the size of ~200 nm are homogeneously dispersed on the Ti_3C_2

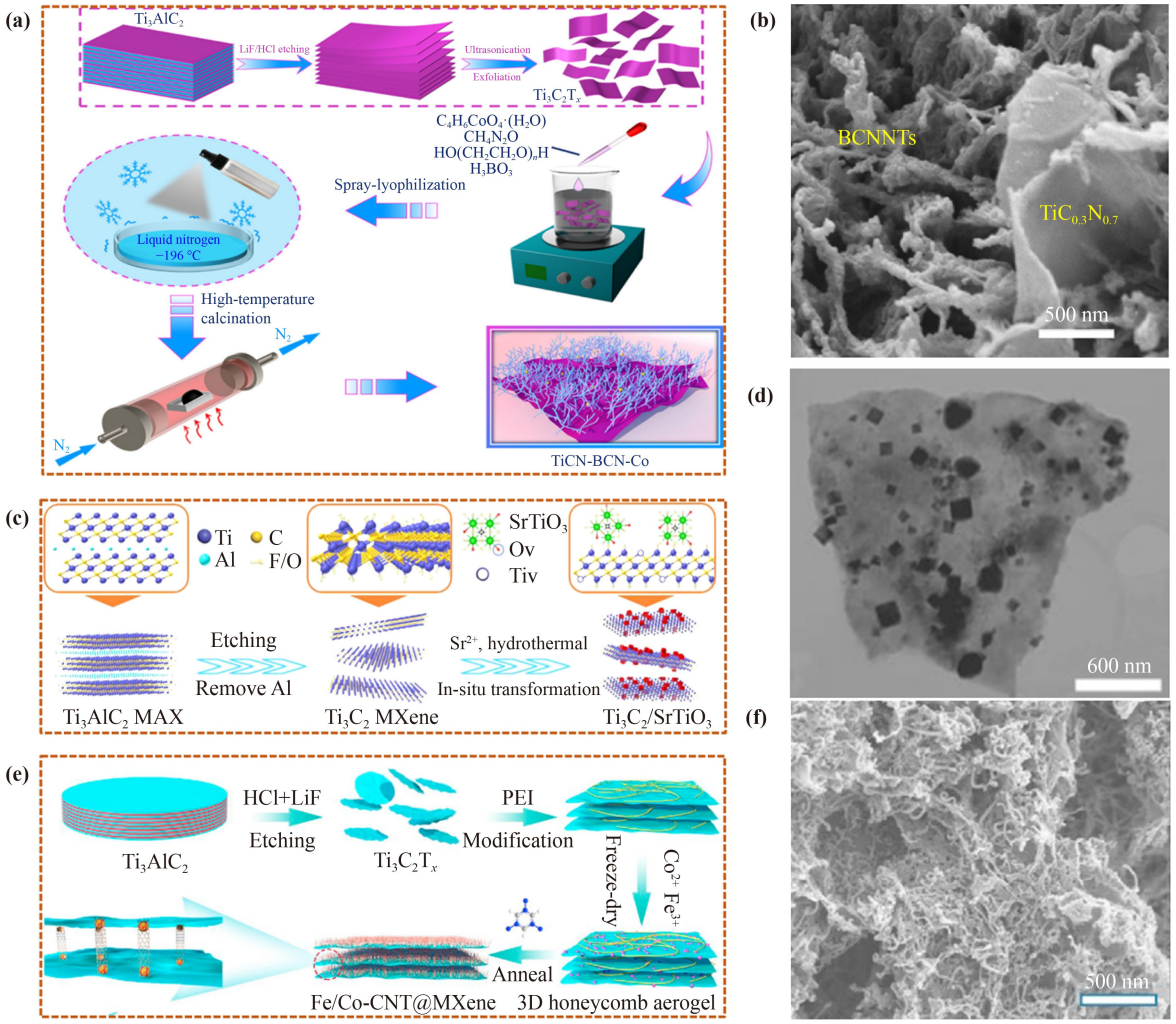

Fig. 3 **(a)** Schematic illustration of the fabrication and **(b)** SEM image of TiCN-BCN-Co. **(c)** Scheme of synthesis and **(d)** TEM image of Ti_3C_2@$SrTiO_3$. **(e)** Schematic illustration of the fabrication and **(f)** SEM image of Fe/Co-CNT@MXene catalyst. (a, b) Reprinted with permission from Ref. [55], Copyright © 2022 Elsevier Ltd. (c, d) Ref. [56] Copyright © 2022 American Chemical Society. (e, f) Ref. [57], Copyright © 2021 Elsevier Ltd.

nanosheets without aggregation, which effectively exposes abundant electrocatalytic active sites. Recently, Ma's group synthesized 3D-structured bifunctional catalysts, where carbon nanotubes (CNTs) decorated with CoFe nanoalloy anchored on 2D MXene (Fe/Co-CNT@MXene) [57]. During the synthesis process [Fig. 3(e)], MXene ($Ti_3C_2T_x$) nanosheets were first produced by etching Ti_3AlC_2 with HCl/LiF under ultrasonic treatment. Then, polyethyleneimine (PEI) solution was dropped into the solution to form a uniform PEI coverage, followed by the addition of $FeCl_3{\cdot}6H_2O$ and $Co(NO_3)_2{\cdot}6H_2O$. After freeze-drying, the prepared 3D honeycomb aerogel was pyrolyzed with melamine to form a final 3D architecture, i.e., FeCo alloy nanoparticles encapsulated by N-doped CNT anchored on the MXene nanosheets. SEM image in Fig. 3(f) reveals the intertwined CNTs anchored on MXene nanosheets with abundant pores and fluffy 3D structures.

3.1.2 Electrocatalytic performance

Since Gogotsi's group first discovered 2D metal carbides and named them as MXenes in 2011 [58], the MXenes family has received extensive attention in the past decade, owing to the special properties [59–61]. This kind of materials especially demonstrates great potential in the application of energy conversion and storage, and also become an outstanding candidate for excellent bifunctional electrocatalyst toward OER/ORR. Qiao's group [62] found that the hybrid film (TCCN) consisting of g-C_3N_4 and Ti_3C_2 nanosheets possesses efficient electrocatalytic activity toward OER as shown in Figs. 4(a) and (b), which originates from the Ti–N_x motifs acting as electroactive sites, and the hierarchically porous structure with highly hydrophilic surface. More importantly, when used in rechargeable ZABs, TCCN displays no obvious potential fluctuation for over 15 pulse cycles, whereas an apparent overpotential increase for both discharging and charging processes is observed after five cycles for IrO_2/C [Fig. 4(c)]. In a recent study, Li *et al.* [63] reported a hybrid electrocatalyst named as FePc-NiCo-LDH/Ti_3C_2, which is engineered by growing of NiCo-LDH in parallel with Ti_3C_2 followed by adsorbing FePc via electrostatic interaction. A good electronic interaction is formed between FePc-NiCo-LDH/Ti_3C_2 and FePc based on MXenes, thereby enhancing the OER activity. The as-prepared bifunctional electrocatalyst exhibits a half-wave potential ($E_{1/2}$) of 80 mV positive compared to Pt/C during the ORR process [Fig. 4(d)] and the overpotential negatively shifts by 89 mV at 10 $mA{\cdot}cm^{-2}$ versus RuO_2 during the OER process [Fig. 4(e)]. In addition, the ZAB assembled with FePc-NiCo-LDH/Ti_3C_2 as air electrode exhibits a peak power density of 148 $mW{\cdot}cm^{-2}$ [Fig. 4(f)] and can be cycled continuously for 80 h.

The development of ORR/OER catalysts for bifunctional activity and long-term durability is critical for the practical application of ZABs. Zhang *et al.* [57] successfully anchored FeCo alloy nanoparticles encapsulated in N-doped carbon nanotubes (CNT) on the surface of N-doped MXene (Fe/CoCNT@MXene-T), where $T{\times}100$ stands for the temperature. The resulting Fe/Co-CNT@MXene-8 catalyst exhibits excellent electrocatalytic activity and high stability to ORR and OER. The ORR linear sweep voltammograms (LSV) exhibit that Fe/CoCNT@MXene-8 has better ORR performance than Pt/C. Moreover, the OER activities of the as-prepared sample and RuO_2 were tested at 10 $mV{\cdot}s^{-1}$ in O_2-saturated 1M KOH solution. Fe/CoCNT@MXene-8 has better OER performance than RuO_2. The specific capacity of ZAB with Fe-Co/CNT@MXene-8 is 18 $mAh{\cdot}g^{-1}$ higher than that Pt/C+RuO_2. After 1000 cycles (350 hours), the ZAB with Fe/Co-CNT@MXene-8 shows a negligible round-trip efficiency ranging from 56.5% to 59.0%. Wei *et al.* [64] proposed an effective solution to search for MXene-based bifunctional catalysts by introducing non-noble metals on the surface. They calculated the activation energy (E_a) of nine Fe/Co/Ni-ACs, which is a decisive factor in determining whether a reaction readily occurs and provides reliable evidence for estimating the reaction rate. Figures 4(g) and (h) show E_a for each step of the ORR and OER. The bar charts show the highest values of the four energy barriers for the nine atomic catalysts (ACs) and the height of the columns represents the reaction barrier in the overall ORR or OER catalytic process. To visualize the bifunctional catalytic properties of catalysts, they calculated the theoretical polarization curves and revealed that the OER and ORR catalytic performances of Ti_2CO_2-based double-atom catalysts (DACs) are very good and close to those of NiO/NC and CoO/NC [Fig. 4(i)]. Some recently reported results about electrocatalytic activity were summarized in Table 1.

MXenes show great potential in the field of energy storage. However, there are still various problems need to be solved in commercial applications. First, compared to graphene, which has similar 2D microstructure to MXenes, it can be mass-produced by CVD or wet chemical etching processes, while MXenes rely on harmful and costly acid-base etchants. Second, due to the highly active surface TM atoms and abundant oxygen-containing functional groups, MXenes are easily oxidized even at room temperature and atmosphere pressure, resulting in the destruction of the crystal structure and a significant decrease in the originally excellent high conductivity, especially in the energy storage device of the water system, which greatly affects the life and performance of the battery.

3.2 Graphene-based electrocatalysts

In the search for potential alternative energy and

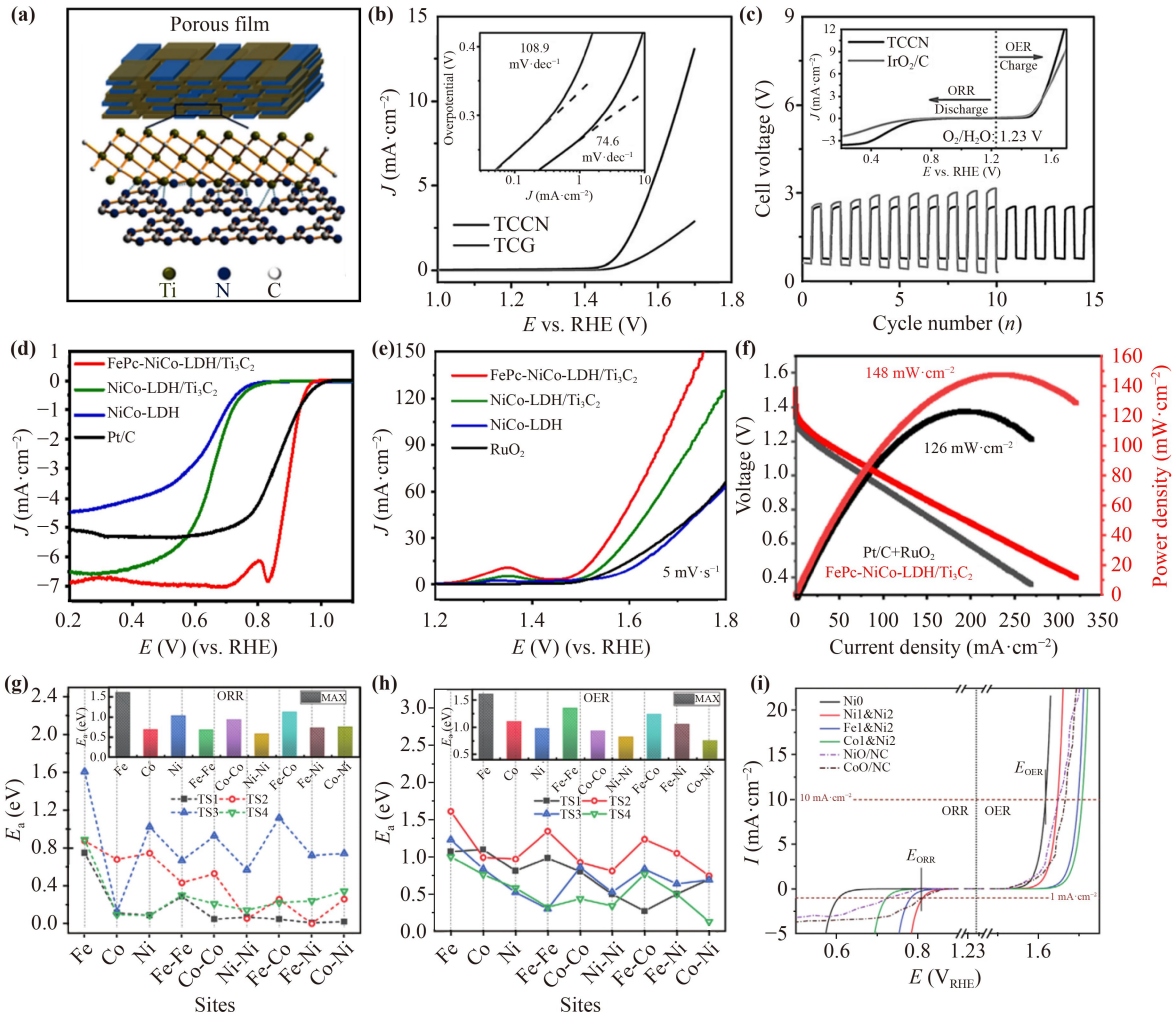

Fig. 4 **(a)** Scheme of TCCN film consisting of g-C_3N_4 and Ti_3C_2 nanosheets, **(b)** polarization curves and Tafel plots of TCCN and TCG, **(c)** charge–discharge cycling curves of a ZAB using the TCCN film and IrO_2/C powder as electrocatalysts in the air cathode, respectively, and (inset) polarization curves of the TCCN film and IrO_2/C powder in the whole OER/ORR region. LSV curves of FePc-NiCo-LDH/Ti_3C_2, NiCo-LDH/Ti_3C_2, NiCo-LDH, and commercial electrocatalyts for **(d)** ORR and **(e)** OER. **(f)** The polarization curves and corresponding power density plots of FePc-NiCo-LDH/Ti_3C_2 and Pt/C+RuO_2 electrodes, respectively. Calculated energy barriers for the kinetic steps and highest energy barrier of the reaction processes in the **(g)** ORR and **(h)** OER. **(i)** Theoretical polarization curves for Ni0-SAC, Ni1&Ni2-DAC, and Fe1&Ni2-DAC and experimental curves for reported bifunctional electrocatalysts (NiO/NC and CoO/NC) in the full range of ORR/OER potentials. (a–c) Reprinted with permission from Ref. [62], Copyright © 2016 Wiley-VCH Verlag GmbH & Co. (d–f) Ref. [63], Copyright © 2022 Elsevier B.V. (g–i) Ref. [64], Copyright © 2021 Wiley-VCH GmbH.

sustainable clean energy, graphene stands out as a superstar in many advanced materials due to its special and important properties. As a carbon allotrope, graphene, with a thickness of only single atomic layer, is composed of sp^2 hybridized carbon atoms, and it is also the basic building block of carbon materials of all other dimensions. It has excellent electrical conductivity and a large specific surface area (~2630 $m^2 \cdot g^{-1}$), in addition to excellent mechanical properties [72] and chemical stability [73]. These special properties make graphene a very promising electrocatalytic material, which is widely used in the field of electrochemical energy storage and conversion [74]. At the same time, due to the regularly repeated structure of graphene, when graphene acts as a template, a uniform composite is often formed, which effectively limits the agglomeration of nanoparticles. Therefore, based on its unique properties, graphene has a wide range of applications in the design and development of ZABs with excellent electrochemical performance.

Perfect graphene usually has no obvious electrocatalytic activity toward ORR/OER. Upon doping heteroatoms or making defects, the modified graphene is endowed with distinct fundamental properties, such as charge redistribution and change of electronic structure, which exhibits outstanding intrinsic activity, because the adsorption energy of oxygen-containing species is accordingly modulated by such modification. Therefore, a range of heteroatoms, including N, S, B, P, O, and

Table 1 Summary of the recent MXene-doped oxygen electrocatalysts reported in the literature.

Materials	OER: $E_{j=10}$ (V vs. RHE) / Overpotential (mV)	ORR: E_{onset} / $E_{1/2}$ (V vs. RHE)	$\Delta E = E_{j=10} - E_{1/2}$ (V)	Open-circuit voltage (V)	Peak power density ($mW \cdot cm^{-2}$)	Specific Capacity ($mAh \cdot g^{-1}$) @ Current density ($mA \cdot cm^{-2}$)	Cycle stability time (h) @ Current density ($mA \cdot cm^{-2}$)	Ref.
CoS_2@MXene	–/270	0.87/0.8	–	1.46	29	–	–	[19]
$SrTiO_3/Ti_3C_2$	–	–/0.78	0.648	1.44	122	789@5	–	[56]
Fe-Co/CNT@MXene-8	–/390	1.02/0.85	0.73	1.41	165	759@10	350@10	[57]
Nb_2CO_2/MXene	–/435	–/0.79	1.09	–	–	–	–	[65]
LDH/MQDs/NG	1.5/–	0.81/0.69	–	1.42	113.8	598@5	150@5	[66]
$H_2PO_2^-$/FeNi-LDH-V_2C	–/250	0.89/0.8	0.673	1.42	–	–	100@5	[67]
NiCoFeLDH/Mxene/NCNT	–/332	0.93/0.78	–	1.54	–	–	–	[68]
$NiCo_2O_4$/MXene	–/310	–/0.7	–	1.4	55.1	–	333@5	[69]
Co_3O_4/2D Ti_3C_2 MXene	1.53/–	–	–	–	–	–	–	[70]
$TiO_2C@CN_{x,950}$	1.50/	–/0.75	0.75	1.344	–	–	48@10	[71]

metal atoms, and various defects (e.g., 5-8-5 defect, 7-55-7 defect) have been explored to improve the performance [75].

3.2.1 Synthesis

Graphene is generally synthesized by either bottom-up method or top-down method. Heteroatom-doped graphene with high electrocatalytic activity is usually obtained via adding heteroatom-containing precursor during the synthesis process. To achieve high performance toward ORR/OER, hybrid electrocatalysts based graphene are often designed and synthesized. Chemical vapor deposition (CVD) is a typical bottom-up method to obtain various heteroatom-doped graphene. Taking N-doped graphene as an example, during the CVD process, carbon-containing and nitrogen-containing precursors are introduced into a tube with a substrate (e.g., Ni metal) to realize the formation of C–C and C–N bond networks at a high temperature (>800 °C). Typically, Zhang *et al.* synthesized a flexible air electrode consisting of 3D nanoporous N-doped graphene with trimodal shells and Ni particles through CVD method and acidic etching processes, as shown in Fig. 5(a) [76]. TEM image in Fig. 5(b) clearly reveals that the Ni particles are coated by few-layer graphene due to the third CVD process. Moreover, the graphene-coated Ni particles are confined into a graphene nanoball, and the graphene nanoball is inside of the nanotubular graphene, resulting in a trimodal nanoporous graphene/Ni composite.

As for top-down method, thermal annealing is a common method to synthesize heteroatom-doped graphene or graphene-based nanocomposites by mixing graphene oxides with heteroatom-containing or transition-metal salts followed by thermal treatment at high temperature. Recently, Ma and coworkers developed a step-by-step self-assembly strategy to allocate Ni and Fe single atoms respectively on the inner and outer walls of graphene hollow nanospheres, as shown in Figs. 5(c) and (d) [26]. Specifically, the positive charged SiO_2 nanospheres was used as templates to adsorb $K_2[Ni(CN)_4]$ and then was encapsulated with graphene oxide (GO) nanosheets to form $SiO_2@[Ni(CN)_4]^{2-}@GO$ nanospheres. Then iron (II) phthalocyanine (FePc) was adsorbed on the nanospheres by π–π stacking interaction. Upon thermal annealing at 700 °C under a flow of N_2 for 3 h and subsequent etching of SiO_2 templates, reduced GO (rGO) hollow spheres with Ni-N_4 and Fe-N_4 active sites were obtained as shown in Fig. 5(d).

Graphene has great potential in interface electronic modulation and electrical conductivity enhancement, but its nearly perfect structure usually causes difficulty to incorporate with other materials. So, some researchers deliberately create defects or modify the surface ligands for functionalizing graphene. Graphitic carbon nitride (g-C_3N_4, CN) provides a good platform to capture and stabilize transition metal ions in ligands, due to the intrinsic mesopores and rich pyridine-like nitrogen, but its electrical conductivity is usually poor due to the large bandgap. Therefore, the combination of graphene and g-C_3N_4, would compensate the drawbacks of each other and form attractive function. For example, the coordination of transition-metal atoms between porous nitrogen-doped graphene and g-C_3N_4 can form a dual-mesh mesoporous single-atomic catalysts [Figs. 6(a, b)] [77]. Three-dimensional nitrogen-doped graphene has high specific surface area and abundant active sites, which effectively captures transition metal atoms and avoids the agglomeration and accumulation of catalysts. Wang *et al.* [78] employed NaCl crystallites as templates to prepare high-performance three-dimensional N-doped graphene. In the process, the freeze-drying homogeneous mixture of polyacrylamide (PAM), Fe-containing salt and NaCl crystal was pyrolyzed under an argon atmosphere. PAM provides abundant N and is fully dissolved in NaCl solution. The Fe precursors coordinate with N to form Fe-N_x active centers. With the decrease of PAM/NaCl mass ratio, the shell opens in the pyrolysis process. When the PAM/NaCl ratio is appropriate (~1:4), the shell has a porous veil-like morphology

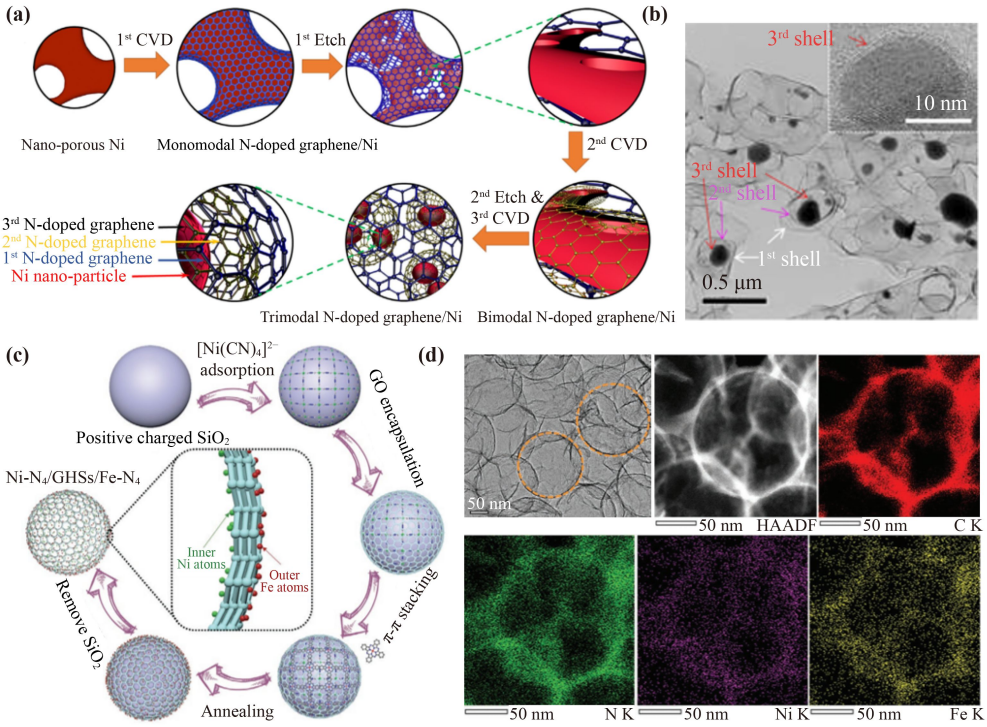

Fig. 5 **(a)** Scheme of the fabrication process of the trimodal N-doped nanoporous graphene/Ni composite and **(b)** TEM image of the final trimodal graphene/Ni composite. **(c)** Synthetic procedure of the Ni-N_4/GHSs/Fe-N_4 catalyst and **(d)** TEM image and elemental mapping. (a, b) Reprinted with permission from Ref. [76], Copyright © 2021 Science Press and Dalian Institute of Chemical Physics, Chinese Academy of Sciences. (c, d) Ref. [77], Copyright © 2020 WILEY-VCH Verlag GmbH & Co.

structure, and the iron atoms are well dispersed in 3D Fe/N-G [Figs. 6(c, d)]. In addition, three-dimensional nitrogen-doped graphene aerogels anchored with transition metal nanoparticles (3D TMNP/N-GAs) can effectively avoid the phenomenon of self-aggregation, and the abundant pores can provide multidimensional electron transport channels [79]. In a typical process [Fig. 6(e)], NiFe-LDH nanosheets were first synthesized via a simple hydrothermal method. Then, the as-prepared NiFe-LDH nanosheets were ultrasonically mixed with a certain amount of pyrrole monomer and GO aqueous solution. Afterwards, rGO/NiFe-LDH/Py aerogel was constructed through a self-assembly hydrothermal method, followed by a vacuum freeze-drying process. Finally, Ni_3Fe-GAs with various nitrogen content were obtained after a thermal treatment at 700 °C in NH_3 or H_2/Ar atmosphere [Fig. 6(f)].

3.2.2 Electrocatalytic performance

Heteroatom-doped (N, S, B, P and halogens) graphene-based materials have received much attention due to their high activity and long-term stability [80–82]. To endow the heteroatom-doped graphene with bifunctional activity towards ORR and OER, transition metal compounds are usually introduced to form nanocomposites [83], where one part plays a dominant role in catalyzing ORR, and the other one catalyzes OER. Wang and coworkers found that the bifunctional activity of CoN_x-graphene stems from moderate hybridization between Co 3d orbital and p-orbital from O species, governed by the neighboring N coordination environment [84]. Tang's group [85] designed 3D graphene aerogel-supported Ni/MnO particles, where MnO mainly contributes to the high activity for the ORR, while metallic Ni is responsible for the excellent OER activity. The as-prepared Ni–MnO/rGO shows a small ΔE of 0.82 V [Fig. 7(a)], demonstrating superior bifunctional eactivity to MnO/rGO and Ni/rGO, which can be attributed to the multi-synergistic effects among metallic Ni, MnO, and 3D porous rGO aerogels [Fig. 7(b)].

A family of hybrid materials comprising amorphous bimetallic oxide nanoparticles ($Fe_aCo_{1-a}Ox$) anchored on N-doped rGO (FeCo/NrGO) with simultaneous control of nanoparticle elemental composition, size, and crystallinity have been synthesized by Chen's group [86]. As shown in Fig. 7(c), the ΔE of optimized $Fe_{0.5}Co_{0.5}O_x$/NrGO hybrid is 0.74 V, which is smaller than that of the Pt/C+IrO_2 mixture (0.78 V). The fabricated Zn–air battery with $Fe_{0.5}Co_{0.5}O_x$/NrGO as electrocatalyst in air electrode delivers a specific capacity of 756 mAh·g_{Zn}^{-1} (corresponding to an energy density of 904 Wh·kg_{Zn}^{-1}), a peak power density of 86 mW·cm^{-2} and can be cycled over 120 h at 10 mA·cm^{-2} [Fig. 7(d)]. Recently, Mai's

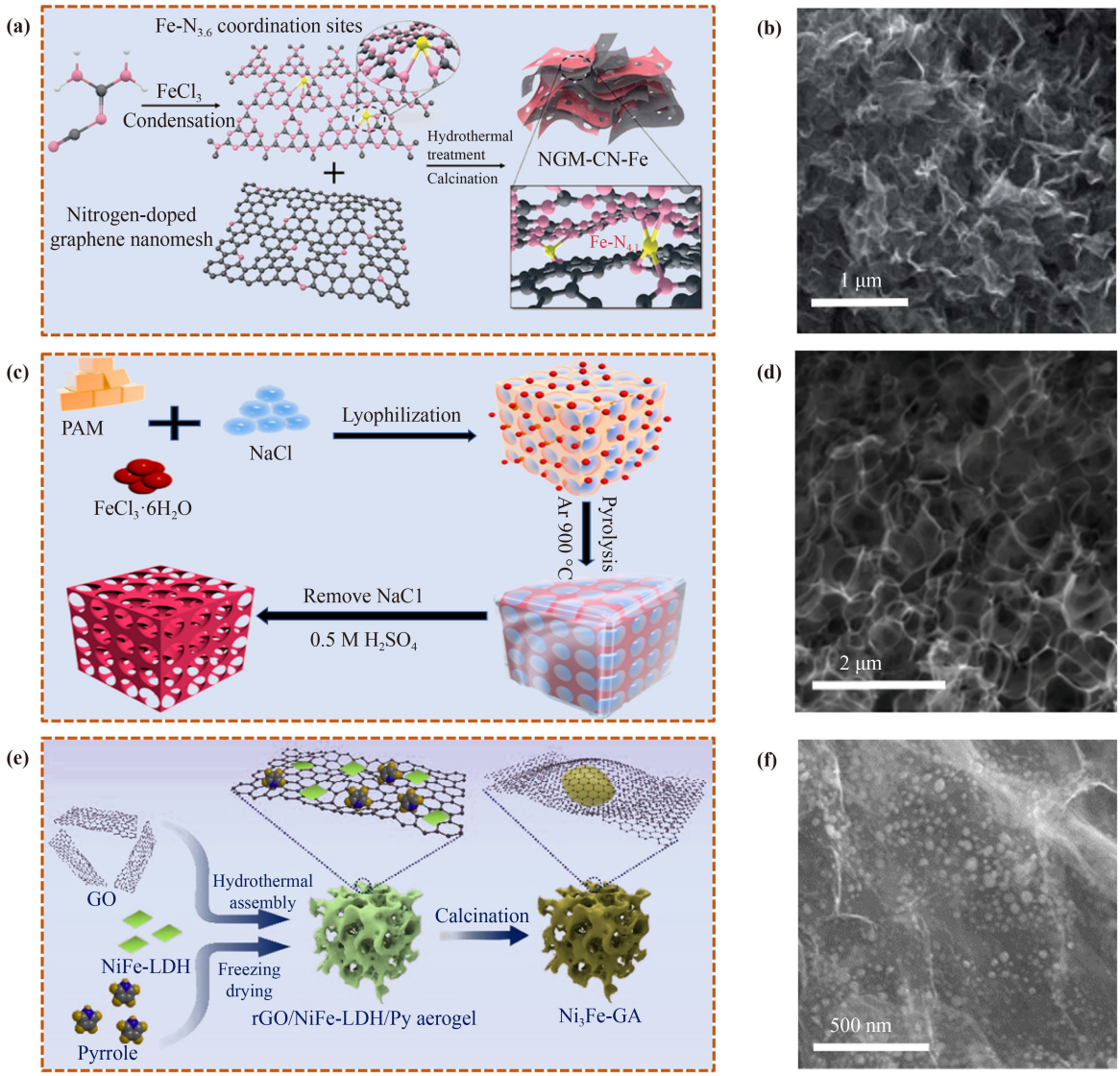

Fig. 6 **(a)** Scheme showing the synthesis of an atomic Fe/g-C_3N_4/graphene nano mesh hybrid electrocatalyst (yellow ball is Fe atom); **(b)** SEM image of NGM–CN–Fe. **(c)** Synthesis Routes of the 3D Fe/N-G Catalysts and **(d)** SEM image of 3D Fe/N-G#4. **(e)** Illustration of the preparation of Ni_3Fe-GA samples and **(f)** SEM image of Ni_3Fe-GA. (a, b) Reprinted with permission from Ref. [78], Copyright © 2019 The Royal Society of Chemistry. (c, d) Ref. [79], Copyright © 2019 American Chemical Society. (e, f) Ref. [80], Copyright © 2020 WILEY-VCH Verlag GmbH & Co.

group [87] developed a series of Ni_3Fe-GA electrocatalysts, one of which exhibits a considerably smaller ΔE of 0.74 V than the mixture of commercial Pt/C and IrO_2 (0.87 V), indicating superior catalytic bifunctionality. The maximum power density of the ZAB equipped with Ni_3Fe-GA catalyst is about 62.9 $mW{\cdot}cm^{-2}$, which is higher than that with Pt/C+IrO_2 mixture (49.6 $mW{\cdot}cm^{-2}$) as shown in Fig. 7(e). The ZAB assembled with Ni_3Fe-GA_1 presents an excellent cycling performance over 100 h (300 cycles) under the condition of galvanostatic charging and discharging at 10 $mA{\cdot}cm^{-2}$ with each cycle spanning 20 min [Fig. 7(f)].

In a recent work reported by Liu *et al.* [88], defect-rich iron/nitrogen co-doped graphene catalytic materials were designed by utilizing ball-milling-induced defects in combination with the $ZnCl_2$ strategy which utilizes mechanically generated scissor force and $ZnCl_2$ corrosion of the carbon matrix, resulting in the generation of large numbers of defects provide favorable conditions for the doping of heteroatoms. The as-prepared electrocatalyt has excellent ORR and OER performance in 0.1M KOH ($E_{1/2}$ = 0.89 V_{RHE}, $E_{j=10}$ = 1.54 V_{RHE}). Wang *et al.* [89] made catalysts with abundant Mott-Schottky non-homogeneous interface by designing a core–shell Mott–Schottky heterostructure (Co_9S_8/Co-rGO) on defect-reduced graphene oxide. This strategy provides multiple guarantees for enhanced electron transfer and ion/oxygen transport, effectively enhancing the catalytic OER and ORR activities in neutral electrolytes. The catalytic material shows highly efficient performance in neutral rechargeable

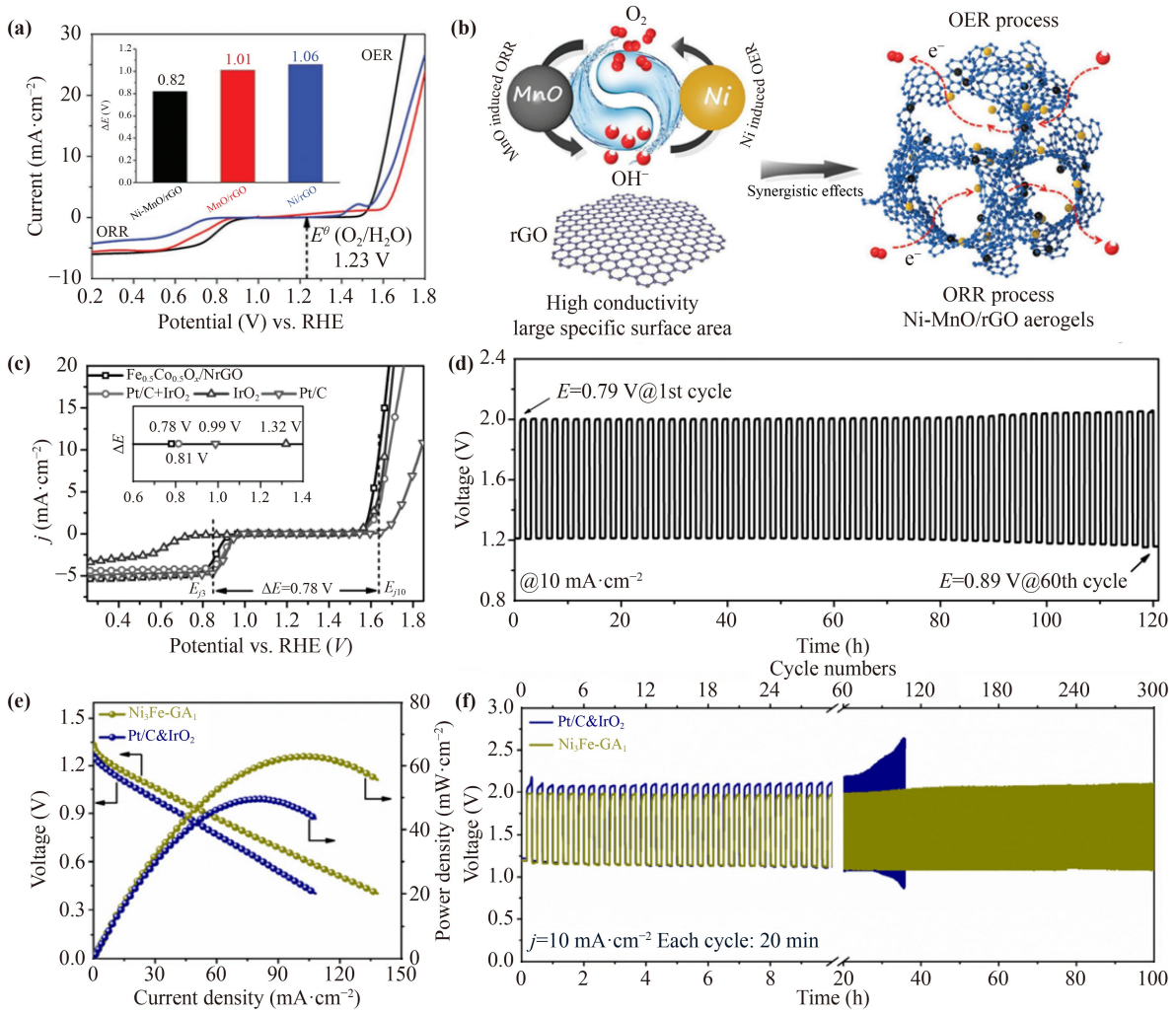

Fig. 7 **(a)** The overall polarization curves of catalysts within the ORR and OER potential window (rotation rate: 1600 rpm; sweep rate: 5 mV·s^{-1}); inset shows the value of ΔE for catalysts; **(b)** Schematic illustration of the compositional and structural advantages of Ni–MnO/rGO as an effcient bifunctional catalyst. **(c)** The ΔE of $Fe_{0.5}Co_{0.5}O_x$/NrGO and mixture of commercial Pt/C and IrO_2. **(d)** Long-term cycling performance at a current density of 10 mA·cm^{-2}, **(e)** Comparison of the discharge polarization and power density curves using Ni_3Fe-GA_1 and Pt/C+IrO_2 as catalysts. **(f)** Galvanostatic charge and discharge cycling curves of Ni_3Fe-GA1 and Pt/C+IrO_2 based ZABs at a current density of 10 mA·cm^{-2}. (a, b) Reprinted with permission from Ref. [85], Copyright © 2017 WILEY-VCH Verlag GmbH & Co. (c, d) Ref. [86], Copyright © 2017 WILEY-VCH Verlag GmbH & Co. KGaA. (e, f) Ref. [87], Copyright ©2020 WILEY-VCH Verlag GmbH & Co.

ZABs with a power density of 59.5 mW·cm^{-2} and the ZAB can be cycled stably for over 200 hours at a current density of 5 mA·cm^{-2}. Defect engineering in transition metal-doped carbon-based catalysts plays a crucial role in improving ORR and OER performances. A relatively detailed comparison of recently reported bifunctional electrocatalysts used in rechargeable ZABs are summarized in Table 2.

3.3 Layered double hydroxides (LDHs)

Layered double hydroxides (LDHs) are a class of metal hydroxides composed of positively charged brucite-like layers and interlayer anions, in addition to water molecules assembled and overlapped by non-covalent bond interactions [100]. The metal cations occupy the centers of edge sharing octahedra, whose vertexes contain hydroxide ions that connect to form infinite 2D sheets. Researchers have been making great efforts to develop efficient LDH-based electrocatalysts over the past decades [101–103]. Thanks to the adjustability of metal cations in the motherboard layer and the properties of anions in the interlayer corridor, the types of metal ions and anions on the laminate can be adjusted according to needs and even be combined with other materials to achieve optimized function [104]. These unique features provide a guarantee for the design of bifunctional electrocatalyst with both high performance and low cost.

Among non-noble metal catalysts, NiFe-layered double hydroxides (NiFe-LDHs) have received extensive

Table 2 Summary of the recent graphene-doped oxygen electrocatalysts reported in the literature.

Materials	OER: $E_{j=10}$ (V vs. RHE)/ Overpotential (mV)	ORR: E_{onset} / $E_{1/2}$ (V vs. RHE)	$\Delta E = E_{j=10} - E_{1/2}$ (V)	Open-circuit voltage (V)	Peak power density ($mW \cdot cm^{-2}$)	Specific Capacity ($mAh \cdot g^{-1}$) @ Current Density ($mA \cdot cm^{-2}$)	Cycle stability time (h) @ Current density ($mA \cdot cm^{-2}$)	Ref.
Co_9S_8/Co–rGO	–/290	0.97/0.79	–	1.34	122	720.1@10	300@5	[89]
AT-Co/NDG	1.54/–	–/0.86	0.68	–	319.8	746.4@50	–	[90]
Trimodal NG/Ni	1.5/270	–/0.86	0.64	1.49	165	743@5	2500@2400@20	[76]
NiFe-Mi-C-Gr	1.535/–	–/0.854	0.681	1.487	111	809@10	102@10	[91]
FeNC/NG-3	–	/0.83	–	1.43	29.5	848.2@10	–	[92]
B-Zn-FeNG	1.54/310	1.03/0.89	0.65	–	229	752@5	80@10	[88]
Ru-RuO_2@NPC	1.45/–	–/0.8	0.65	1.43	137	–	–	[24]
CoS/CoO@NGNs	1.61/	–/0.84	0.77	–	137.8	711.1@20	100@10	[93]
CoDNG900	1.614/	0.943/0.864	0.75	1.45	205	669@10	667@10	[94]
NSP-Gra	1.76	–	0.94	–	225	–	40@215@5	[95]
Fe-N-C/2rGO	1.56/	–/0.88	0.68	1.47	164	–	30@10	[96]
Co_3O_4–$NiCo_2O_4$ /N-RGO	1.62/390	–/0.79	0.83	1.49	97	–	180@290@10	[97]
FeCoNi-N-rGO	1.67/	–/0.836	0.834	1.43	152.5	766@5	200@5	[98]
CN@NC-2-800	1.66/400	–/0.83	0.83	1.52	172	806.9@10	300@10	[99]

research attention, particularly, owing to the remarkable OER performance arising from the transformation of LDH to the (oxy)hydroxide phase [105–109]. Mhin and coworkers investigated such transformation by DFT calculations and electrochemical experiments [110]. They found that the phase transformation of NiFe-LDH (Fe: 38 at.%) to $Ni_{1-x}Fe_xOOH$ is thermodynamically spontaneous under the applied $U = 1.23$ V in the alkaline condition, pH = 14. More importantly, besides the phase transformation, there are usually oxyanions intercalated or absorbed at the surface of $Ni_{1-x}Fe_xOOH$, which can affect the electronic properties of catalyst and improve the electrocatalytic activity [111]. For example, Li *et al.* [112] found that residual PO_4^{3-} ions induce redistribution of electron states, and optimize the adsorption of OH* and OOH* intermediates on metal oxyhydroxides and promoting the OER activity. Moreover, NiOOH-PO_x shows optimal local coordination environment and boosts electrocatalytic activity of Ni sites towards selective oxidation of methanol to formate [101].

3.3.1 Synthesis

Layered double hydroxides and corresponding oxyhydroxides have attracted considerable research attention, mainly owing to the unique layered structure and outstanding catalytic activity. The intrinsic activities of LDHs and oxyhydroxides are closely related to the number of the 3d electrons in Ni–Fe atoms. And the e_g orbitals which can bind with the surface adsorbates and thus affecting the binding of oxygen intermediates [113]. The introduction of third transition metal into LDHs is the most common way to adjust the electronic structure and improve the catalytic performance, such as CoNiFe-LDH. The synthetic methods of LDHs are usually facile and scalable. In a typical process [Figs. 8(a, b)] [114], 3 mmol $Ni(NO_3)_2 \cdot 6H_2O$, 1 mmol $Fe(NO_3)_3 \cdot 9H_2O$, 10 mmol NH_4F and 25 mmol urea were co-dissolved in 50 mL of deionized water under stirring, NiFe-LDH was prepared by centrifugation and washing with deionized water and ethanol, after heating in a Teflon autoclave. CoNiFe-LDH can be prepared by adding Co precursor under the same procedure as the preparation of NiFe-LDH. In contrast, $Co(OH)_2$ nanoarray-deposited NiFe-LDH (Co@NiFe-LDH) can be obtained by changing the procedure. Typically, the preparation of Co@NiFe-LDH should avoid Co doping via the etching process and ionic exchange. The prepared NiFe-LDH was immersed vertically into 50 mL solution containing 1 mmol $Co(NO_3)_2 \cdot 6H_2O$, 10 mmol NH_4F, and 25 mmol urea, and kept stirring for 20 min. Then the mixture was transferred into an autoclave and heated at 120 °C for 10 h. The final product was collected after rinsed for several times and centrifuged.

Structural engineering strategies supported by carbon cloth have been widely used in the preparation of high-efficiency oxygen catalysts. The fabrication of self-supporting electrocatalysts will effectively avoid loss of porosity and activity due to multiple functions as both catalytic active sites and collectors. In the process, ZIF-L-Co precursors were placed upstream of the tubular furnace with 0.1 g of dicyanamide. It was then annealed at 400 °C for 2 hours and heated to 750 °C for 2 hours to obtain Co@NC-CNTs. The prepared material is immersed in an aqueous solution containing $Ni(NO_3)_2 \cdot 6H_2O$, $Fe(NO_3)_3 \cdot 9H_2O$ and urea. The mixture was then transferred to an Teflon-lined autoclave at 120 °C for three hours, and the product was treated with deionized water several times to obtain Co@NC-CNTs@NiFe-LDH [Figs. 8(c, d)] [115]. In addition, the hierarchical hollow heterostructure is characterized to have abundant active centers and high specific surface area, which can effectively

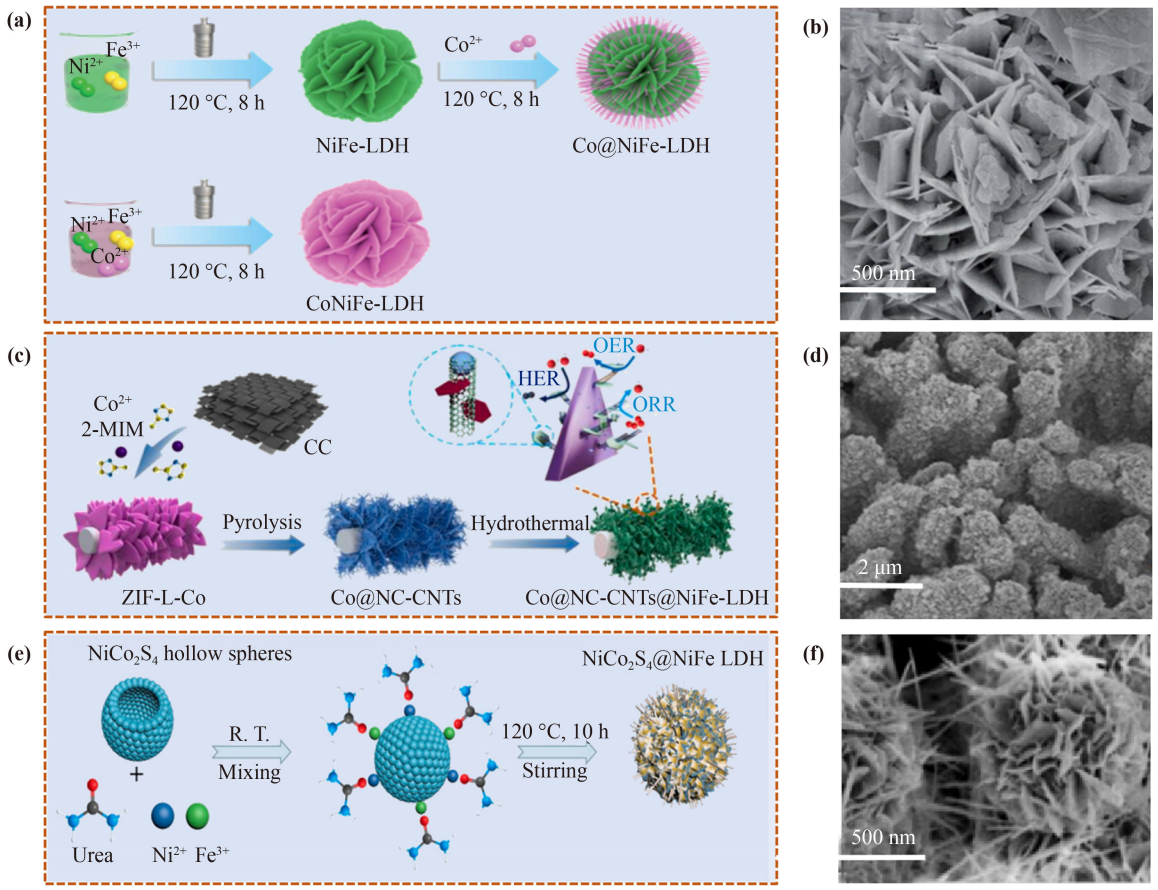

Fig. 8 **(a)** Schematic illustration for synthesizing NiFe-LDH, CoNiFe-LDH, and Co@NiFe-LDH nanosheet flowers. **(b)** SEM images of) Co@NiFe-LDH nanosheet flowers. **(c)** Schematic illustration of the formation of the Co@NC-CNTs@NiFe-LDH electrocatalyst. SEM image of the **(d)** Co@NC-CNTs@NiFe-LDH samples. **(e)** Schematic diagram for the $NiCo_2S_4$@NiFe LDH. and SEM image **(f)** of the $NiCo_2S_4$@NiFe LDH. (a, b) Reprinted with permission from Ref. [114], Copyright © 2022 The Royal Society of Chemistry. (c, d) Ref. [115], Copyright © 2022 Elsevier B.V. All rights reserved. (e, f) Ref. [116], Copyright © 2021 Elsevier B.V. All rights reserved.

expand the interface between catalyst and electrolyte and achieve fast ion/electron transport. Feng *et al.* [116] reported a facile strategy for preparing cactus-like $NiCo_2S_4$@NiFe LDH hollow spheres. Briefly, 0.5 mmol $Fe(NO_3)_3{\cdot}9H_2O$, 5 mmol urea and 1.5 mmol $Ni(NO_3)_2{\cdot}6H_2O$ were completely dissolved in 50 mL distilled water by magnetic stirring, and 100 mg $NiCo_2S_4$ hollow spheres were added and stirred continuously for 1 h. The prepared solution was poured into 75 mL Teflon-lined autoclave and kept at 120 °C in a continuously rolled oven for 10 hours. Finally, the solid products were washed with water and ethanol, and dried at 60 °C overnight [Figs. 8(e, f)].

3.3.2 Electrocatalytic performance

As promising OER electrocatalysts, layered double hydroxides (LDHs) have also been widely studied to be used in the rechargeable ZABs [63, 117]. To realize the bifunctional electrocatalysis toward OER and ORR, LDHs are usually hybridized with other materials with good ORR performance or modified by other strategies [118]. Li's group [119] synthesized nanocomposites (NiCo-NS/rGO) consisting of CoNi-LDH monolayers and reduced graphene oxide and obtained good activity and stability far more superior to its competitors (Pt/C and Ir/C) for ORR/OER in both 1 M and 6 M KOH as shown in Figs. 9(a) and (b). When discharged galvanostatically at 10 or 50 $mA{\cdot}cm^{-2}$, the ZAB with CoNi-NS/rGO outputs a voltage of 1.25 V and 1.06 V, respectively, which maintain stable during 8–12 h under the continuous operation [Fig. 9(c)].

Doping with heteroatoms is also a good strategy to endow NiFe-LDH-based electrocatalysts with bifunctional activity. In a recent work [120], NiFe-LDH was grown in situ on Fe and N atoms-modified carbon nanofibers by electrospinning and hydrothermal reaction, which achieves efficient OER and ORR properties. The LDH clusters with thin-layered structures grow uniformly on the carbon nanofibers. The three-dimensional grid structure promotes the stability of the cathode, and provides abundant reaction sites, which significantly improves the catalytic efficiency and conductivity under the synergistic effect of NiFe-LDH. This bifunctional electrocatalyst

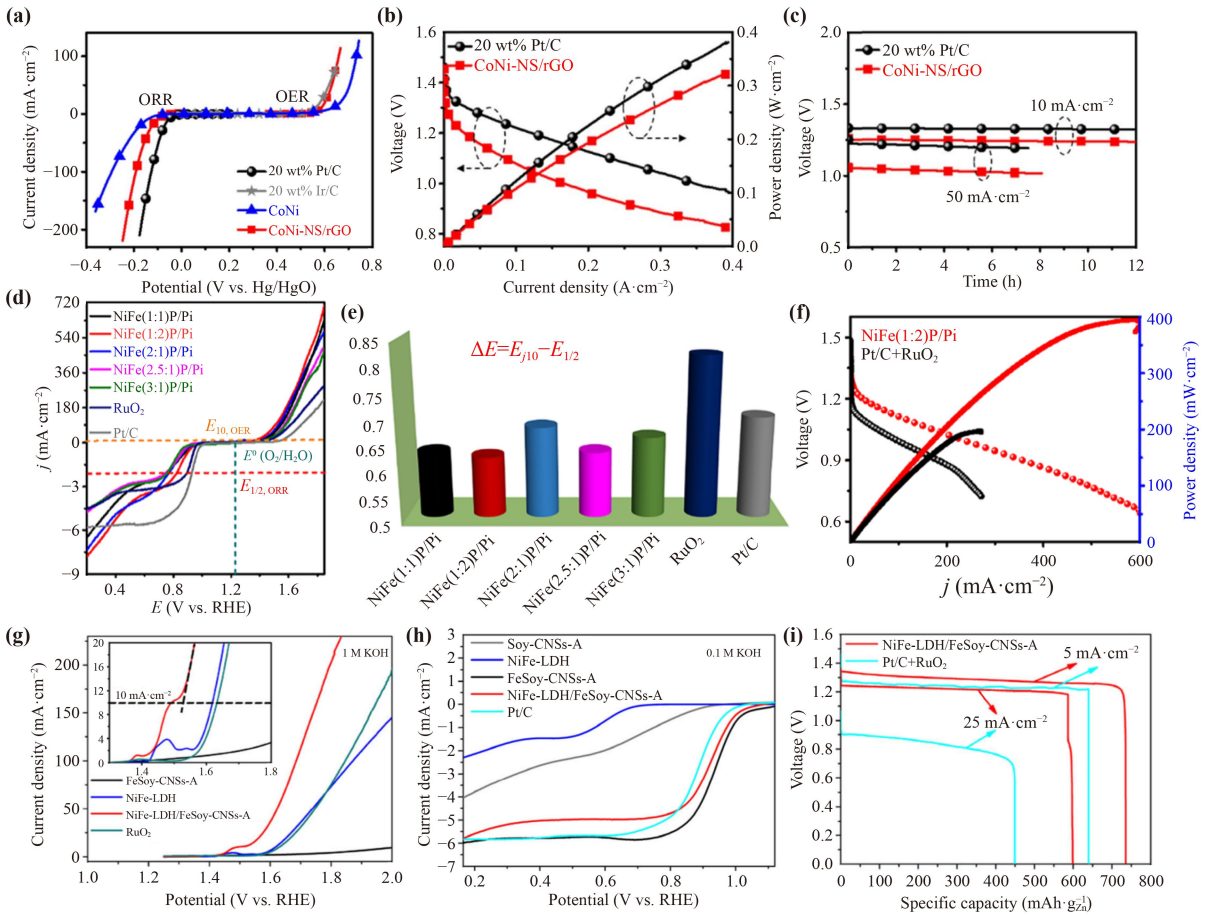

Fig. 9 **(a)** ORR and OER polarization curves of CoNi-LDH (CoNi) and CoNi-LDH nanosheets coupled with rGO (CoNi-NS/rGO); **(b)** Discharge polarization curve and corresponding power density of Zn–air batteries using CoNi-NS/rGO or Pt/C as the oxygen catalyst; and **(c)** galvanostatic discharge curves of Zn–air batteries using CoNi-NS/rGO or Pt/C as the oxygen catalyst at 10 or 50 mA·cm^{-2}, **(d)** LSV curves of both the OER and ORR of various catalysts, **(e)** bar diagram representing the potential difference of OER and ORR as the oxygen bifunctional catalyst; **(f)** power density plots and discharge curves at 10 mA·cm^{-2} of the Zn–air battery using the NiFe(1:2)P/Pi air cathode; LSV profiles during the ORR **(g)** and OER **(h)** process, respectively, for Soy-CNSs-A, NiFe-LDH, FeSoy-CNSs-A, NiFe-LDH/FeSoy-CNSs-A and Pt/C; **(i)** The galvanostatic discharge curves of the ZABs using NiFe-LDH/FeSoy-CNSs-A and Pt/C+RuO_2 catalysts as air electrode at the current density of 5 and 25 mA·cm^{-2}, respectively. (a–c) Reprinted with permission from Ref. [119], Copyright © 2018 Published by Elsevier B.V. (d–f) Reprinted with permission from Ref. [123], Copyright © 2021 American Chemical Society. (g–i) Reprinted with permission from Ref. [124], Copyright ©2020 Tsinghua University Press and Springer-Verlag GmbH Germany, part of Springer Nature.

possesses excellent activity for ORR/OER with the difference of potential (ΔE = 0.86 V) between $E_{j\,=\,10}$ and $E_{1/2}$. Moreover, the prepared rechargeable Zn–air battery also has high specific capacity (695.2 mAh·g^{-1}) and energy density (838.6 Wh·kg$^{-1}_{Zn}$), which can remain a stable duration of 184 h at a current of 10 mA·cm^{-2}. In addition, Zhou *et al.* [121] modulated the electronic structure of NiFe-LDHs by introducing foreign metals, the Mn^{2+} ions with high reductivity and weak electronegativity activating the base surface of NiFe-LDHs to enhance OER activity. Recently, Jia *et al.* [122] developed a controlled atomic defect engineering method and demonstrated that the introduction of defects into the catalyst can significantly improve its catalytic efficiency. The as-prepared $Ni_{1/2}Fe_{1/2}(OH)_2$/CNT catalyst was able to provide a remarkably small overpotential of 244 mV at 10 mA·cm^{-2} for the OER in 1 M KOH solution. Thakur *et al.* [123] treated the firstly prepared NiFe-LDH with different Ni/Fe ratios by low-temperature phosphorization reaction and obtained various phosphide/phosphate (NiFeP/Pi) catalysts. The optimized NiFe(1:2)P/Pi exhibits a low OER overpotential of 0.21 V at 10 mA·cm^{-2} and a high ORR onset potential (0.98 V vs. RHE) with the lowest ΔE of 0.62 V [Figs. 9(d, e)]. The rechargeable ZAB with NiFe(1:2)P/Pi demonstrates a very high power density of 395 mW·cm^{-2}, which surpasses the counterpart with the benchmark Pt/C and RuO_2 [Fig. 9(f)].

Zhang *et al.* [124] combined ultrathin NiFe-LDH nanowalls with a renewable soybean-derived Fe-N-C matrix

to obtain a hybrid material (NiFe-LDH/FeSoy-CNSs-A). NiFe-LDH/FeSoy-CNSs-A was obtained by in situ and vertical immobilization of ultra-small NiFe-LDH nanosheets on a low-cost soybean-derived high-conductivity Fe-N-C substrate via a co-precipitation strategy. The as-prepared material exhibits remarkable OER activity [Fig. 9(g)] and superior ORR activity [Fig. 9(h)] with the ΔE of only 0.62 V, which is much lower than that of the benchmark Pt/C+RuO_2. In addition, NiFe-LDH/FeSoy-CNSs-A exhibits a much lower charge/discharge voltage gap (ΔE = 0.74 V) at a high current density of 100 mA·cm^{-2}. Moreover, the NiFe-LDH/FeSoy-CNSs-A-based battery showed superhigh capacities (735 mAh·g$^{-1}_{Zn}$ at 5 mA·cm^{-2} and 600 mAh·g$^{-1}_{Zn}$ at 25 mA·cm^{-2}) by normalizing it to the mass of consumed Zn [Fig. 9(i)]. Wang *et al.* [125] deposited NiFe-LDH particles on Co, N-codoped carbon nanoframes (Co, N-CNFs) and assembled ZAB by utilizing Co, N-CNFs as bifunctional electrocatalyst in air electrode. Based on the high conductivity and excellent ORR activity of Co with N-CNF, the assembled ZAB exhibited long-term cycling stability (over 80 hours) and low discharge-charge voltage gap (1.0 V at 25 mA·cm^{-2}). In addition, layered nickel-iron-cobalt nanosheets/carbon fibers (NiFeCo-LDH/CF) were synthesized by solvothermal treatment using ZIF-67/CF [126], and it was shown that the substitution of Co can stabilize the local environment of Fe. The π-symmetrical bonding orbitals of NiFeCo-LDH/CF are effectively promoted, while a large number of active surface sites and CF ensure the transfer of charges after the electronic structure is changed, which effectively promotes the OER activity of the material.

The progress of LDHs materials has greatly promoted the development of the field of energy storage, especially the continuous improvement of rechargeable ZABs (Table 3). The development of catalysts with excellent OER and ORR performance favors to shorten the commercialization process of zinc–air batteries. However, there are still some key issues to be solved in practical applications. OER/ORR performance can be effectively improved by heteroatom doping, defect engineering and introduction of the third metal element. Therefore, the development of scalable synthetic methods and cost-effective catalytic materials is the current main task.

3.4 Others

The preparation of catalytic materials with excellent bifunctional properties is not limited to the above three aspects. TM dichalcogenide (TMD) nanosheets, such as MoS_2, WS_2, $MoSe_2$ and WSe_2, have received considerable attention due to their unique structures and excellent properties. The single-atom functionalization of TMD nanosheets is a powerful strategy for the design of catalytic with excellent properties. The ORR performance is inactive for the pristine TMDs, unless doping with TMs or non-metal substitutional atoms. For example, Meza *et al.* [131] anchored single Ni atom on WS_2 nanosheet and the catalyst shows good performance for OER. Theoretically, Tian *et al.* [132] found that single Ni and Co atom can perform as eligible ORR electrocatalysts when anchored on TiS_2, ZrS_2, TaS_2, and NbS_2. Doping with TMs and non-metal substitutional atoms successfully endow the electrocatalysts with superior performance towrad OER or ORR, but it is hard to achieve materials with excellent bifunctional properties. Qin *et al.* [133] found that Ni@VS_2 exhibits good catalytic performance for both OER and ORR under the low overpotentials (0.45 and 0.31 V) through the comprehensive density functional theory (DFT) computations. More interestingly, when introducing a certain number of N dopants into the VS_2 substrate, the ORR/OER catalytic activity can be further enhanced.

Metal-organic frameworks (MOFs) are frequently used as a precursor to developing MOF-derived electrode catalysts, which not only retain the advantages of the original structure but also provide enhanced conductivity and stability [42]. Compared with 3D MOFs, 2D MOFs exhibits better in electrocatalysis in terms of active sites and electron transport. In addition, 2D MOFs materials have the properties of inorganic 2D materials and mild synthesis. Moreover, the large numbers of organic ligands cause the unique physical and chemical properties of 2D MOFs [134]. In 2016, Tang *et al.* [135] for the first time reported that ultrathin 2D NiCo-MOF nanosheets loaded on nickel foam exhibit remarkable stability for at least 200 h in the electrocatalytic OER, and the material can reach an overpotential of 250 mV at 10 mA·cm^{-2} [135]. Based on this enlightening work, a large number of high-efficiency electrocatalysts have been synthesized and applied. Huang *et al.* [136] found a pillared-layer

Table 3 ORR/OER activity and zinc-air battery performance of various kinds of reported materials based on NiFe-LDH.

Air catalyst	Electrolyte	$E_{j=10}$	$E_{1/2}$	ΔE ($E_{j=10}$–$E_{1/2}$)	Cycles or time (h) @ Current density (mA·cm^{-2})	Ref.
NiFe(1:2)P/Pi	KOH	–	–	0.62V	300 cycles@10	[123]
NiFe-LDH/FeSoy-CNSs-A	KOH	1.53V	0.91V	0.62V	300 cycles@5	[124]
nNiFe LDH/3D MPC	KOH	1.572V	0.862V	0.71V	100 cycles@10	[127]
Cu@Cu NWs@LDH	KOH	1.44V	0.719V	0.721V	240 h@10	[128]
CoNC@LDH	KOH	1.47V	0.84V	0.63V	3600 cycles@10	[129]
$NiCo_2O_4$@FeNi LDH/Ni	KOH	–	–	–	90 h@10	[130]

MOF based on coordination bonds, and the electrocatalyst exhibits a low overpotential and high turnover frequency. Li *et al.* [137] reported the design and synthesis of Co@N-C700 which can be facilely achieved on a large scale, and the rechargeable ZAB assembled with the material delivers a steady discharge voltage plateau of 1.22 V within 240 h.

4 Conclusion and outlook

With the increasing demand for energy conversion devices in modern society, electrocatalysts play a decisive role in the performance of ZABs. To improve the performance and durability of ZABs, it is of urgent significance to explore efficient oxygen electrocatalysts. Researchers have adopted different approaches in the design of oxygen electrocatalysts, the essence of which is to design low-cost, high-performance catalytic materials for the commercial development of ZABs. Based on a brief introduction to the principles of ZABs, this review introduces the research on the bifunctional performance of typical 2D materials-based electrocatalysts, including LDHs, graphene, and MXenes. Despite the great achievements in the field of ZABs, there are still many challenges, especially the design and scalable synthesis of efficient electrocatalytic materials. The synthesis and electrocatalytic performance are the prerequisites of practical application (Fig. 10). Meanwhile, 2D electrocatalysts provide an ideal platform for the in-situ/operando characterization as well as theoretical calculations to gain in-depth understanding on the electrocatalytic mechanism. The combination of experiments and simulation will clearly reveal the structure-property relationships, which is beneficial for the practical application of rechargeable ZABs [138, 139]. In addition, the performance, safety and cost aspects also need to be further balanced. It is essential to study high-performance bifunctional electrocatalyst toward oxygen electrocatalysis by optimizing the materials design and exploring new schemes.

The current mainstream heteroatom doping and defect engineering have a positive impact on the design of high-performance electrode materials, and greatly promote the preparation of bifunctional oxygen catalysts. Benefiting from the rapid development of big data and computational power, data-driven machine learning has become a powerful tool to screen and predict high-performance electrocatalysts. On the other hand, the in-situ or operando characterization techniques start playing a more and more important role in revealing the electrocatalytic mechanism, which is also very helpful for the design of advanced electrocatalyst. Among many materials, 2D materials with large specific surface area and good electrical conductivity stand out from many potential candidates for bifunctional electrocatalysts, which will open a new avenue for the future applications in rechargeable ZABs.

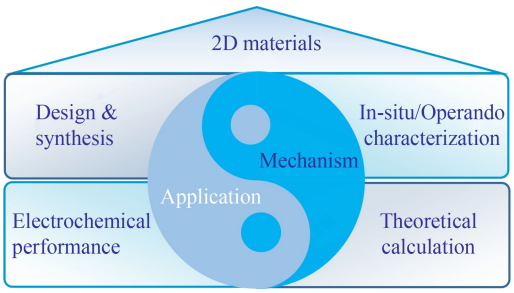

Fig. 10 Schematic illustration of future study on 2D materials as bifunctional oxygen electrocatalysts in rechargeable ZABs.

Acknowledgements This work was supported by the Fundamental Research Funds for Central Universities and the National Key R&D Program of China (Grant No. 2016YFC1402504), and also partially supported by grants from the National Natural Science Foundation of China (No. 52172058).

References

1. J. Han and H. Chang, Development and opportunities of clean energy in China, *Appl. Sci. (Basel)* 12(9), 4783 (2022)
2. L. S. Martins, L. F. Guimarães, A. B. Botelho Junior, J. A. S. Tenório, and D. C. R. Espinosa, Electric car battery: An overview on global demand, recycling and future approaches towards sustainability, *J. Environ. Manage.* 295, 113091 (2021)
3. N. O. Moraga, J. P. Xamán, and R. H. Araya, Cooling Li-ion batteries of racing solar car by using multiple phase change materials, *Appl. Therm. Eng.* 108, 1041 (2016)
4. D. A. Notter, M. Gauch, R. Widmer, P. Wäger, A. Stamp, R. Zah, and H. J. Althaus, Contribution of Li-ion batteries to the environmental impact of electric vehicles, *Environ. Sci. Technol.* 44(17), 6550 (2010)
5. X. Zeng, J. Li, and L. Liu, Solving spent lithium-ion battery problems in China: Opportunities and challenges, *Renew. Sustain. Energy Rev.* 52, 1759 (2015)
6. H. Jiao, S. Jiao, W. L. Song, X. Xiao, D. She, N. Li, H. Chen, J. Tu, M. Wang, and D. Fang, Al homogeneous deposition induced by N-containing functional groups for enhanced cycling stability of Al-ion battery negative electrode, *Nano Res.* 14(3), 646 (2021)
7. J. Li, Z. Kong, X. Liu, B. Zheng, Q. H. Fan, E. Garratt, T. Schuelke, K. Wang, H. Xu, and H. Jin, Strategies to anode protection in lithium metal battery: A review, *InfoMat* 3(12), 1333 (2021)
8. S. Chen, Z. Gao, and T. Sun, Safety challenges and safety measures of Li-ion batteries, *Energy Sci. Eng.* 9(9), 1647 (2021)
9. D. P. Finegan, J. Zhu, X. Feng, M. Keyser, M. Ulmefors, W. Li, M. Z. Bazant, and S. J. Cooper, The application of data-driven methods and physics-based learning for improving battery safety, *Joule* 5(2), 316 (2021)

10. B. Xu, J. Lee, D. Kwon, L. Kong, and M. Pecht, Mitigation strategies for Li-ion battery thermal runaway: A review, *Renew. Sustain. Energy Rev.* 150, 111437 (2021)
11. M. Abbas, I. Cho, and J. Kim, Scalable constrained attributes/issues about risk, reliability and optimization in large scale battery pack, *J. Energy Storage* 39, 102632 (2021)
12. G. Kovachev, A. Astner, G. Gstrein, L. Aiello, J. Hemmer, W. Sinz, and C. Ellersdorfer, Thermal conductivity in aged Li-ion cells under various compression conditions and state-of-charge, *Batteries* 7(3), 42 (2021)
13. H. Liu, Q. Liu, Y. Wang, Y. Wang, S. Chou, Z. Hu, and Z. Zhang, Bifunctional carbon-based cathode catalysts for zinc-air battery: A review, *Chin. Chem. Lett.* 33(2), 683 (2022)
14. W. Li, W. Chen, H. Zhang, and Z. Zhang, Integratable solid-state zinc–air battery with extended cycle life inspired by bionics, *Chem. Eng. J.* 435, 134900 (2022)
15. A. R. Mainar, E. Iruin, and J. A. Blázquez, High performance secondary zinc-air/silver hybrid battery, *J. Energy Storage* 33, 102103 (2021)
16. S. Wang, S. Chen, L. Ma, and J. A. Zapien, Recent progress in cobalt-based carbon materials as oxygen electrocatalysts for zinc–air battery applications, *Mater. Today Energy* 20, 100659 (2021)
17. J. Zhou, L. Shan, Z. Wu, X. Guo, G. Fang, and S. Liang, Investigation of V_2O_5 as a low-cost rechargeable aqueous zinc ion battery cathode, *Chem. Commun.* 54, 4457 (2018)
18. K. Jayasayee, S. Clark, C. King, P. I. Dahl, J. Richard Tolchard, and M. Juel, Cold sintering as a cost-effective process to manufacture porous zinc electrodes for rechargeable zinc-air batteries, *Processes (Basel)* 8(5), 592 (2020)
19. S. Han, Y. Chen, Y. Hao, Y. Xie, D. Xie, Y. Chen, Y. Xiong, Z. He, F. Hu, L. Li, J. Zhu, and S. Peng, Multidimensional hierarchical CoS2@MXene as trifunctional electrocatalysts for zinc-air batteries and overall water splitting, *Sci. China Mater.* 64(5), 1127 (2021)
20. J. Huang, Y. Xie, L. Yan, B. Wang, T. Kong, X. Dong, Y. Wang, and Y. Xia, Decoupled amphoteric water electrolysis and its integration with Mn–Zn battery for flexible utilization of renewables, *Energy Environ. Sci.* 14(2), 883 (2021)
21. C. Zhou, X. Chen, S. Liu, Y. Han, H. Meng, Q. Jiang, S. Zhao, F. Wei, J. Sun, T. Tan, and R. Zhang, Superdurable bifunctional oxygen electrocatalyst for high-performance zinc–air batteries, *J. Am. Chem. Soc.* 144(6), 2694 (2022)
22. C. Han, W. Li, H. K. Liu, S. Dou, and J. Wang, Design strategies for developing non-precious metal based bi-functional catalysts for alkaline electrolyte based zinc–air batteries, *Mater. Horiz.* 6(9), 1812 (2019)
23. Z. Chen, J. Y. Choi, H. Wang, H. Li, and Z. Chen, Highly durable and active non-precious air cathode catalyst for zinc air battery, *J. Power Sources* 196(7), 3673 (2011)
24. N. Wang, S. Ning, X. Yu, D. Chen, Z. Li, J. Xu, H. Meng, D. Zhao, L. Li, Q. Liu, B. Lu, and S. Chen, Graphene composites with Ru-RuO_2 heterostructures: Highly efficient Mott–Schottky-type electrocatalysts for pH-universal water splitting and flexible zinc–air batteries, *Appl. Catal. B* 302, 120838 (2022)
25. Q. Zhu, Y. Qu, D. Liu, K. W. Ng, and H. Pan, Two-dimensional layered materials: High-efficient electrocatalysts for hydrogen evolution reaction, *ACS Appl. Nano Mater.* 3(7), 6270 (2020)
26. L. Yu, F. Li, J. Zhao, and Z. Chen, Revisiting catalytic performance of supported metal dimers for oxygen reduction reaction via magnetic coupling from first principles, *Adv. Powder Mater.* 1(3), 100031 (2022)
27. C. Xia, Y. Zhou, C. He, A. I. Douka, W. Guo, K. Qi, and B. Y. Xia, Recent advances on electrospun nanomaterials for zinc–air batteries, *Small Sci.* 1(9), 2100010 (2021)
28. Z. Zhang, H. Zhang, Y. Yao, J. Wang, H. Guo, Y. Deng, and X. Han, Controlled synthesis and structure engineering of transition metal-based nanomaterials for oxygen and hydrogen electrocatalysis in zinc-air battery and water-splitting devices, *ChemSusChem* 14(7), 1659 (2021)
29. Z. Zhang, Y. Tan, T. Zeng, L. Yu, R. Chen, N. Cheng, S. Mu, and X. Sun, Tuning the dual-active sites of ZIF-67 derived porous nanomaterials for boosting oxygen catalysis and rechargeable Zn–air batteries, *Nano Res.* 14(7), 2353 (2021)
30. D. Ren, J. Ying, M. Xiao, Y. P. Deng, J. Ou, J. Zhu, G. Liu, Y. Pei, S. Li, A. M. Jauhar, H. Jin, S. Wang, D. Su, A. Yu, and Z. Chen, Hierarchically porous multimetal-based carbon nanorod hybrid as an efficient oxygen catalyst for rechargeable zinc–air batteries, *Adv. Funct. Mater.* 30(7), 1908167 (2020)
31. H. Sun, M. Wang, S. Zhang, S. Liu, X. Shen, T. Qian, X. Niu, J. Xiong, and C. Yan, Boosting oxygen dissociation over bimetal sites to facilitate oxygen reduction activity of zinc–air battery, *Adv. Funct. Mater.* 31(4), 2006533 (2021)
32. X. Zhong, S. Ye, J. Tang, Y. Zhu, D. Wu, M. Gu, H. Pan, and B. Xu, Engineering Pt and Fe dual-metal single atoms anchored on nitrogen-doped carbon with high activity and durability towards oxygen reduction reaction for zinc–air battery, *Appl. Catal. B* 286, 119891 (2021)
33. J. Han, H. Bao, J. Q. Wang, L. Zheng, S. Sun, Z. L. Wang, and C. Sun, 3D N-doped ordered mesoporous carbon supported single-atom Fe-N-C catalysts with superior performance for oxygen reduction reaction and zinc–air battery, *Appl. Catal. B* 280, 119411 (2021)
34. X. Han, T. Zhang, W. Chen, B. Dong, G. Meng, L. Zheng, C. Yang, X. Sun, Z. Zhuang, D. Wang, A. Han, and J. Liu, Mn-N_4 oxygen reduction electrocatalyst: Operando investigation of active sites and high performance in zinc–air battery, *Adv. Energy Mater.* 11(6), 2002753 (2021)
35. W. Wu, Y. Liu, D. Liu, W. Chen, Z. Song, X. Wang, Y. Zheng, N. Lu, C. Wang, J. Mao, and Y. Li, Single copper sites dispersed on hierarchically porous carbon for improving oxygen reduction reaction towards zinc–air battery, *Nano Res.* 14(4), 998 (2021)
36. J. Zhang, Q. Zhou, Y. Tang, L. Zhang, and Y. Li, Zinc–air batteries: are they ready for prime time,

Chem. Sci. (Camb.) 10(39), 8924 (2019)
37. M. Wu, Y. Wang, Z. Wei, L. Wang, M. Zhuo, J. Zhang, X. Han, and J. Ma, Ternary doped porous carbon nanofibers with excellent ORR and OER performance for zinc–air batteries, *J. Mater. Chem. A* 6(23), 10918 (2018)
38. Y. Zheng, Y. Jiao, Y. Zhu, Q. Cai, A. Vasileff, L. H. Li, Y. Han, Y. Chen, and S. Z. Qiao, Molecule-level g-C_3N_4 coordinated transition metals as a new class of electrocatalysts for oxygen electrode reactions, *J. Am. Chem. Soc.* 139(9), 3336 (2017)
39. C. Han, W. Li, H. K. Liu, S. Dou, and J. Wang, Design strategies for developing non-precious metal based bi-functional catalysts for alkaline electrolyte based zinc–air batteries, *Mater. Horiz.* 6(9), 1812 (2019)
40. X. Cai, L. Lai, J. Lin, and Z. Shen, Recent advances in air electrodes for Zn–air batteries: Electrocatalysis and structural design, *Mater. Horiz.* 4(6), 945 (2017)
41. Y. Li and H. Dai, Recent advances in zinc–air batteries, *Chem. Soc. Rev.* 43(15), 5257 (2014)
42. Y. Zhu, K. Yue, C. Xia, S. Zaman, H. Yang, X. Wang, Y. Yan, and B. Y. Xia, Recent advances on MoF derivatives for non-noble metal oxygen electrocatalysts in zinc–air batteries, *Nano-Micro Lett.* 13(1), 137 (2021)
43. M. Shao, Q. Chang, J. P. Dodelet, and R. Chenitz, Recent advances in electrocatalysts for oxygen reduction reaction, *Chem. Rev.* 116(6), 3594 (2016)
44. T. Reier, M. Oezaslan, and P. Strasser, Electrocatalytic oxygen evolution reaction (OER) on Ru, Ir, and Pt catalysts: A comparative study of nanoparticles and bulk materials, *ACS Catal.* 2(8), 1765 (2012)
45. S. Huang, J. Zhu, J. Tian, and Z. Niu, Recent progress in the electrolytes of aqueous zinc-ion batteries, *Chemistry* 25(64), 14480 (2019)
46. J. Hao, X. Li, S. Zhang, F. Yang, X. Zeng, S. Zhang, G. Bo, C. Wang, and Z. Guo, Designing dendrite-free zinc anodes for advanced aqueous zinc batteries, *Adv. Funct. Mater.* 30(30), 2001263 (2020)
47. Y. Zhang, G. Yang, M. L. Lehmann, C. Wu, L. Zhao, T. Saito, Y. Liang, J. Nanda, and Y. Yao, Separator effect on zinc electrodeposition behavior and its implication for zinc battery lifetime, *Nano Lett.* 21(24), 10446 (2021)
48. R. Qin, G. Shan, M. Hu, and W. Huang, Two-dimensional transition metal carbides and/or nitrides (MXenes) and their applications in sensors, *Mater. Today Physics* 21, 100527 (2021)
49. K. Li, M. Liang, H. Wang, X. Wang, Y. Huang, J. Coelho, S. Pinilla, Y. Zhang, F. Qi, V. Nicolosi, and Y. Xu, 3D MXene architectures for efficient energy storage and conversion, *Adv. Funct. Mater.* 30(47), 2000842 (2020)
50. J. Wang, C. F. Du, Y. Xue, X. Tan, J. Kang, Y. Gao, H. Yu, and Q. Yan, MXenes as a versatile platform for reactive surface modification and superior sodium-ion storages, *Exploration* 1(2), 20210024 (2021)
51. K. Li, M. Liang, H. Wang, X. Wang, Y. Huang, J. Coelho, S. Pinilla, Y. Zhang, F. Qi, V. Nicolosi, and Y. Xu, 3D MXene architectures for efficient energy storage and conversion, *Adv. Funct. Mater.* 30(47), 2000842 (2020)
52. X. Zhang, J. Xu, H. Wang, J. Zhang, H. Yan, B. Pan, J. Zhou, and Y. Xie, Ultrathin nanosheets of MAX phases with enhanced thermal and mechanical properties in polymeric compositions: $Ti_3Si_{0.75}Al_{0.25}C_2$, *Angew. Chem. Int. Ed.* 52(16), 4361 (2013)
53. J. Halim, M. R. Lukatskaya, K. M. Cook, J. Lu, C. R. Smith, L. A. Näslund, S. J. May, L. Hultman, Y. Gogotsi, P. Eklund, and M. W. Barsoum, Transparent conductive two-dimensional titanium carbide epitaxial thin films, *Chem. Mater.* 26(7), 2374 (2014)
54. C. Xu, L. Wang, Z. Liu, L. Chen, J. Guo, N. Kang, X. L. Ma, H. M. Cheng, and W. Ren, Large-area high-quality 2D ultrathin Mo_2C superconducting crystals, *Nat. Mater.* 14(11), 1135 (2015)
55. Y. Wang, F. Gu, L. Cao, L. Fan, T. Hou, Q. Zhu, Y. Wu, and S. Xiong, TiCN MXene hybrid BCN nanotubes with trace level Co as an efficient ORR electrocatalyst for Zn-air batteries, *Int. J. Hydrogen Energy* 47(48), 20894 (2022)
56. X. Hui, P. Zhang, Z. Wang, D. Zhao, Z. Li, Z. Zhang, C. Wang, and L. Yin, Vacancy defect-rich perovskite $SrTiO_3/Ti_3C_2$ heterostructures in situ derived from Ti_3C_2 MXenes with exceptional oxygen catalytic activity for advanced Zn–air batteries, *ACS Appl. Energy Mater.* 5(5), 6100 (2022)
57. C. Zhang, H. Dong, B. Chen, T. Jin, J. Nie, and G. Ma, 3D MXene anchored carbon nanotube as bifunctional and durable oxygen catalysts for Zn–air batteries, *Carbon* 185, 17 (2021)
58. M. Naguib, M. Kurtoglu, V. Presser, J. Lu, J. Niu, M. Heon, L. Hultman, Y. Gogotsi, and M. W. Barsoum, Two-dimensional nanocrystals produced by exfoliation of Ti_3AlC_2, *Adv. Mater.* 23(37), 4248 (2011)
59. W. Zaman, R. A. Matsumoto, M. W. Thompson, Y. H. Liu, Y. Bootwala, M. B. Dixit, S. Nemsak, E. Crumlin, M. C. Hatzell, P. T. Cummings, and K. B. Hatzell, *In situ* investigation of water on MXene interfaces, *Proc. Natl. Acad. Sci. USA* 118(49), e2108325118 (2021)
60. T. Zhou, C. Wu, Y. Wang, A. P. Tomsia, M. Li, E. Saiz, S. Fang, R. H. Baughman, L. Jiang, and Q. Cheng, Super-tough MXene-functionalized graphene sheets, *Nat. Commun.* 11(1), 2077 (2020)
61. R. Qin, M. Hu, X. Li, T. Liang, H. Tan, J. Liu, and G. Shan, A new strategy for the fabrication of a flexible and highly sensitive capacitive pressure sensor, *Microsyst. Nanoeng.* 7(1), 100 (2021)
62. T. Y. Ma, J. L. Cao, M. Jaroniec, and S. Z. Qiao, Interacting carbon nitride and titanium carbide nanosheets for high-performance oxygen evolution, *Angew. Chem. Int. Ed.* 55(3), 1138 (2016)
63. G. L. Li, S. Cao, Z. F. Lu, X. Wang, Y. Yan, and C. Hao, FePc nanoclusters modified NiCo layered double hydroxides in parallel with Ti_3C_2 MXene as a highly efficient and durable bifunctional oxygen electrocatalyst for zinc–air batteries, *Appl. Surf. Sci.* 591, 153142 (2022)
64. B. Wei, Z. Fu, D. Legut, T. C. Germann, S. Du, H. Zhang, J. S. Francisco, and R. Zhang, Rational design of highly stable and active MXene-based bifunctional ORR/OER double-atom catalysts, *Adv. Mater.* 33(40), 2102595 (2021)
65. H. Zong, W. Liu, M. Li, S. Gong, K. Yu, and Z. Zhu, Oxygen-terminated Nb_2CO_2 MXene with interfacial

self-assembled COF as a bifunctional catalyst for durable zinc–air batteries, *ACS Appl. Mater. Interfaces* 14(8), 10738 (2022)
66. X. Han, N. Li, P. Xiong, M. G. Jung, Y. Kang, Q. Dou, Q. Liu, J. Y. Lee, and H. S. Park, Electronically coupled layered double hydroxide/ MXene quantum dot metallic hybrids for high-performance flexible zinc–air batteries, *InfoMat* 3(10), 1134 (2021)
67. Y. Chen, H. Yao, F. Kong, H. Tian, G. Meng, S. Wang, X. Mao, X. Cui, X. Hou, and J. Shi, V_2C MXene synergistically coupling FeNi LDH nanosheets for boosting oxygen evolution reaction, *Appl. Catal. B* 297, 120474 (2021)
68. M. Faraji and N. Arianpouya, NiCoFe-layered double hydroxides/MXene/N-doped carbon nanotube composite as a high performance bifunctional catalyst for oxygen electrocatalytic reactions in metal–air batteries, *J. Electroanal. Chem. (Lausanne)* 901, 115797 (2021)
69. H. Lei, S. Tan, L. Ma, Y. Liu, Y. Liang, M. S. Javed, Z. Wang, Z. Zhu, and W. Mai, Strongly coupled $NiCo_2O_4$ nanocrystal/MXene hybrid through *in situ* Ni /Co–F bonds for efficient wearable Zn–air batteries, *ACS Appl. Mater. Interfaces* 12(40), 44639 (2020)
70. Y. Lu, D. Fan, Z. Chen, W. Xiao, C. Cao, and X. Yang, Anchoring Co_3O_4 nanoparticles on MXene for efficient electrocatalytic oxygen evolution, *Sci. Bull. (Beijing)* 65(6), 460 (2020)
71. L. He, J. Liu, Y. Liu, B. Cui, B. Hu, M. Wang, K. Tian, Y. Song, S. Wu, Z. Zhang, Z. Peng, and M. Du, Titanium dioxide encapsulated carbon–nitride nanosheets derived from MXene and melamine-cyanuric acid composite as a multifunctional electrocatalyst for hydrogen and oxygen evolution reaction and oxygen reduction reaction, *Appl. Catal. B* 248, 366 (2019)
72. A. Fasolino, J. H. Los, and M. I. Katsnelson, Intrinsic ripples in graphene, *Nat. Mater.* 6(11), 858 (2007)
73. A. A. Balandin, S. Ghosh, W. Bao, I. Calizo, D. Teweldebrhan, F. Miao, and C. N. Lau, Superior thermal conductivity of single-layer graphene, *Nano Lett.* 8(3), 902 (2008)
74. I. Y. Jeon, M. J. Ju, J. Xu, H. J. Choi, J. M. Seo, M. J. Kim, I. T. Choi, H. M. Kim, J. C. Kim, J. J. Lee, H. K. Liu, H. K. Kim, S. Dou, L. Dai, and J. B. Baek, Edge-fluorinated graphene nanoplatelets as high performance electrodes for dye-sensitized solar cells and lithium ion batteries, *Adv. Funct. Mater.* 25(8), 1170 (2015)
75. Y. Jia, L. Zhang, A. Du, G. Gao, J. Chen, X. Yan, C. L. Brown, and X. Yao, Defect graphene as a trifunctional catalyst for electrochemical reactions, *Adv. Mater.* 28(43), 9532 (2016)
76. Y. Zhang, X. P. Kong, X. Lin, K. Hu, W. Zhao, G. Xie, X. Lin, X. Liu, Y. Ito, and H. J. Qiu, Enhanced bifunctional catalytic activities of N-doped graphene by Ni in a 3D trimodal nanoporous nanotubular network and its ultralong cycling performance in Zn-air batteries, *J. Energy Chem.* 66, 466 (2022)
77. C. Wang, H. Zhao, J. Wang, Z. Zhao, M. Cheng, X. Duan, Q. Zhang, J. Wang, and J. Wang, Atomic Fe hetero-layered coordination between g-C_3N_4 and graphene nanomeshes enhances the ORR electrocatalytic performance of zinc–air batteries, *J. Mater. Chem. A* 7(4), 1451 (2019)
78. C. Wang, Z. Li, L. Wang, X. Niu, and S. Wang, Facile synthesis of 3D Fe/N codoped mesoporous graphene as efficient bifunctional oxygen electrocatalysts for rechargeable Zn–air batteries, *ACS Sustain. Chem. & Eng.* 7(16), 13873 (2019)
79. Z. Wang, X. Liao, Z. Lin, F. Huang, Y. Jiang, K. A. Owusu, L. Xu, Z. Liu, J. Li, Y. Zhao, Y. B. Cheng, and L. Mai, 3D nitrogen-doped graphene encapsulated metallic nickel-iron alloy nanoparticles for efficient bifunctional oxygen electrocatalysis, *Chemistry* 26(18), 3896 (2020)
80. L. Qin, L. Wang, X. Yang, R. Ding, Z. Zheng, X. Chen, and B. Lv, Synergistic enhancement of oxygen reduction reaction with BC_3 and graphitic-N in boron- and nitrogen-codoped porous graphene, *J. Catal.* 359, 242 (2018)
81. L. L. Tian, J. Yang, M. Y. Weng, R. Tan, J. X. Zheng, H. B. Chen, Q. C. Zhuang, L. M. Dai, and F. Pan, Fast diffusion of O_2 on nitrogen-doped graphene to enhance oxygen reduction and its application for high-rate Zn–air batteries, *ACS Appl. Mater. Interfaces* 9(8), 7125 (2017)
82. J. Zhang, H. Zhou, J. Zhu, P. Hu, C. Hang, J. Yang, T. Peng, S. Mu, and Y. Huang, Facile synthesis of defect-rich and S/N Co-doped graphene-like carbon nanosheets as an efficient electrocatalyst for primary and all-solid-state Zn–air batteries, *ACS Appl. Mater. Interfaces* 9(29), 24545 (2017)
83. S. Wu, D. Deng, E. Zhang, H. Li, and L. Xu, CoN nanoparticles anchored on ultra-thin N-doped graphene as the oxygen reduction electrocatalyst for highly stable zinc-air batteries, *Carbon* 196, 347 (2022)
84. X. Zhang, Z. Yang, Z. Lu, and W. Wang, Bifunctional CoNx embedded graphene electrocatalysts for OER and ORR: A theoretical evaluation, *Carbon* 130, 112 (2018)
85. G. Fu, X. Yan, Y. Chen, L. Xu, D. Sun, J. M. Lee, and Y. Tang, Boosting bifunctional oxygen electrocatalysis with 3D graphene aerogel-supported Ni/MnO particles, *Adv. Mater.* 30(5), 1704609 (2018)
86. L. Wei, H. E. Karahan, S. Zhai, H. Liu, X. Chen, Z. Zhou, Y. Lei, Z. Liu, and Y. Chen, Amorphous bimetallic oxide–graphene hybrids as bifunctional oxygen electrocatalysts for rechargeable Zn–air batteries, *Adv. Mater.* 29(38), 1701410 (2017)
87. Z. Wang, X. Liao, Z. Lin, F. Huang, Y. Jiang, K. A. Owusu, L. Xu, Z. Liu, J. Li, Y. Zhao, Y. B. Cheng, and L. Mai, 3D nitrogen-doped graphene encapsulated metallic nickel–iron alloy nanoparticles for efficient bifunctional oxygen electrocatalysis, *Chem.* 26(18), 4044 (2020)
88. Y. Liu, J. Bao, Z. Li, L. Zhang, S. Zhang, L. Wang, X. Niu, P. Sun, and L. Xu, Large-scale defect-rich iron/ nitrogen co-doped graphene-based materials as the excellent bifunctional electrocatalyst for liquid and flexible all-solid-state zinc–air batteries, *J. Colloid Interface Sci.* 607, 1201 (2022)
89. X. Wang, G. Zhan, Y. Wang, Y. Zhang, J. Zhou, R. Xu, H. Gai, H. Wang, H. Jiang, and M. Huang, Engineering core–shell Co9S8/Co nanoparticles on reduced graphene oxide: Efficient bifunctional Mott–Schottky electrocatalysts in neutral rechargeable Zn–air batteries, *J. Energy Chem.* 68, 113 (2022)

90. X. Shu, M. Yang, M. Liu, W. Pan, and J. Zhang, The regulation of coordination structure between cobalt and nitrogen on graphene for efficient bifunctional electrocatalysis in Zn–air batteries, *J. Energy Chem.* 68, 213 (2022)
91. Y. Xiang, C. Xu, T. Fu, Y. Tang, G. Li, Z. Xiong, C. Guo, and Y. Si, Enhanced bifunctional catalytic performance of nitrogen-doped carbon composite to oxygen reduction and evolution reactions with the regulation of graphene for rechargeable Zn–air batteries, *Appl. Surf. Sci.* 575, 151730 (2022)
92. T. Wang, J. Feng, Q. Liu, X. Han, and D. Wu, Facile synthesis of amino acids-derived Fe/N-codoped reduced graphene oxide for enhanced ORR electrocatalyst, *J. Electroanal. Chem. (Lausanne)* 915, 116326 (2022)
93. Y. Tian, L. Xu, M. Li, D. Yuan, X. Liu, J. Qian, Y. Dou, J. Qiu, and S. Zhang, Interface engineering of CoS/CoO@N-doped graphene nanocomposite for high-performance rechargeable Zn–air batteries, *Nano-Micro Lett.* 13(1), 3 (2021)
94. A. Wang, C. Zhao, M. Yu, and W. Wang, Trifunctional Co nanoparticle confined in defect-rich nitrogen-doped graphene for rechargeable Zn-air battery with a long lifetime, *Appl. Catal. B* 281, 119514 (2021)
95. Y. Wang, N. Xu, R. He, L. Peng, D. Cai, and J. Qiao, Large-scale defect-engineering tailored tri-doped graphene as a metal-free bifunctional catalyst for superior electrocatalytic oxygen reaction in rechargeable Zn–air battery, *Appl. Catal. B* 285, 119811 (2021)
96. X. Zhao, L. Shao, Z. Wang, H. Chen, H. Yang, and L. Zeng, *In situ* atomically dispersed Fe doped metal-organic framework on reduced graphene oxide as bifunctional electrocatalyst for Zn–air batteries, *J. Mater. Chem. C* 9(34), 11252 (2021)
97. Z. Zhu, J. Zhang, X. Peng, Y. Liu, T. Cen, Z. Ye, and D. Yuan, Co_3O_4–$NiCo_2O_4$ hybrid nanoparticles anchored on N-doped reduced graphene oxide nanosheets as an efficient catalyst for Zn–air batteries, *Energy Fuels* 35(5), 4550 (2021)
98. X. Chen, D. Chen, G. Li, C. Gong, Y. Chen, Q. Zhang, J. Sui, H. Dong, J. Yu, L. Yu, and L. Dong, A hierarchical architecture of Fe/Co/Ni-doped carbon nanotubes/nanospheres grafted on graphene as advanced bifunctional electrocatalyst for Zn–air batteries, *J. Alloys Comp.* 873, 159833 (2021)
99. Z. Zhu, Q. Xu, Z. Ni, K. Luo, Y. Liu, and D. Yuan, CoNi nanoalloys @ N-doped graphene encapsulated in n-doped carbon nanotubes for rechargeable Zn–air batteries, *ACS Sustain. Chem. & Eng.* 9(40), 13491 (2021)
100. Q. Wang and D. O'Hare, Recent advances in the synthesis and application of layered double hydroxide (LDH) nanosheets, *Chem. Rev.* 112(7), 4124 (2012)
101. S. Li, R. Ma, J. Hu, Z. Li, L. Liu, X. Wang, Y. Lu, G. E. Sterbinsky, S. Liu, L. Zheng, J. Liu, D. Liu, and J. Wang, Coordination environment tuning of nickel sites by oxyanions to optimize methanol electro-oxidation activity, *Nat. Commun.* 13(1), 2916 (2022)
102. Y. Zhao, X. Zhang, X. Jia, G. I. N. Waterhouse, R. Shi, X. Zhang, F. Zhan, Y. Tao, L. Z. Wu, C. H. Tung, D. O'Hare, and T. Zhang, Sub-3 nm ultrafine monolayer layered double hydroxide nanosheets for electrochemical water oxidation, *Adv. Energy Mater.* 8(18), 1703585 (2018)
103. G. Chen, H. Wan, W. Ma, N. Zhang, Y. Cao, X. Liu, J. Wang, and R. Ma, Layered metal hydroxides and their derivatives: Controllable synthesis, chemical exfoliation, and electrocatalytic applications, *Adv. Energy Mater.* 10(11), 1902535 (2020)
104. K. Yan, G. Wu, and W. Jin, Recent advances in the synthesis of layered, double-hydroxide-based materials and their applications in hydrogen and oxygen evolution, *Energy Technol. (Weinheim)* 4(3), 354 (2016)
105. S. Dresp, F. Luo, R. Schmack, S. Kühl, M. Gliech, and P. Strasser, An efficient bifunctional two-component catalyst for oxygen reduction and oxygen evolution in reversible fuel cells, electrolyzers and rechargeable air electrodes, *Energy Environ. Sci.* 9(6), 2020 (2016)
106. C. Tang, H. S. Wang, H. F. Wang, Q. Zhang, G. L. Tian, J. Q. Nie, and F. Wei, Spatially confined hybridization of nanometer-sized NiFe hydroxides into nitrogen-doped graphene frameworks leading to superior oxygen evolution reactivity, *Adv. Mater.* 27(30), 4516 (2015)
107. M. Gong, Y. Li, H. Wang, Y. Liang, J. Z. Wu, J. Zhou, J. Wang, T. Regier, F. Wei, and H. Dai, An advanced Ni–Fe layered double hydroxide electrocatalyst for water oxidation, *J. Am. Chem. Soc.* 135(23), 8452 (2013)
108. M. Salmanion and M. M. Najafpour, Dendrimer-Ni-based material: Toward an efficient Ni–Fe layered double hydroxide for oxygen-evolution reaction, *Inorg. Chem.* 60(8), 6073 (2021)
109. J. Zhang, L. Yu, Y. Chen, X. F. Lu, S. Gao, and X. W. D. Lou, Designed formation of double-shelled Ni–Fe layered-double-hydroxide nanocages for efficient oxygen evolution reaction, *Adv. Mater.* 32(16), 1906432 (2020)
110. K. R. Park, J. Jeon, H. Choi, J. Lee, D. H. Lim, N. Oh, H. Han, C. Ahn, B. Kim, and S. Mhin, NiFe layered double hydroxide electrocatalysts for an efficient oxygen evolution reaction, *ACS Appl. Energy Mater.* 5(7), 8592 (2022)
111. J. N. Hausmann and P. W. Menezes, Effect of surface-adsorbed and intercalated (Oxy)anions on the oxygen evolution reaction, *Angew. Chem. Int. Ed.* 61(38), e202207279 (2022)
112. S. Li, Z. Li, R. Ma, C. Gao, L. Liu, L. Hu, J. Zhu, T. Sun, Y. Tang, D. Liu, and J. Wang, A glass-ceramic with accelerated surface reconstruction toward the efficient oxygen evolution reaction, *Angew. Chem. Int. Ed.* 60, 3773 (2021)
113. C. Wei, Z. Feng, G. G. Scherer, J. Barber, Y. Shao-Horn, and Z. J. Xu, Cations in octahedral sites: A descriptor for oxygen electrocatalysis on transition-metal spinels, *Adv. Mater.* 29(23), 1606800 (2017)
114. S. Liu, R. Wan, Z. Lin, Z. Liu, Y. Liu, Y. Tian, D. D. Qin, and Z. Tang, Probing the Co role in promoting the OER and Zn–air battery performance of NiFe-LDH: A combined experimental and theoretical study, *J. Mater. Chem. A* 10(10), 5244 (2022)
115. L. Yan, Z. Xu, X. Liu, S. Mahmood, J. Shen, J. Ning, S. Li, Y. Zhong, and Y. Hu, Integrating trifunctional Co@NC-CNTs@NiFe-LDH electrocatalysts with arrays of porous triangle carbon plates for high-power-density

rechargeable Zn–air batteries and self-powered water splitting, *Chem. Eng. J.* 446, 137049 (2022)
116. X. Feng, Q. Jiao, W. Chen, Y. Dang, Z. Dai, S. L. Suib, J. Zhang, Y. Zhao, H. Li, and C. Feng, Cactus-like $NiCo_2S_4$@NiFe LDH hollow spheres as an effective oxygen bifunctional electrocatalyst in alkaline solution, *Appl. Catal. B* 286, 119869 (2021)
117. Z. Kong, J. Chen, X. Wang, X. Long, X. She, D. Li, and D. Yang, Cation vacancy driven efficient CoFe-LDH-based electrocatalysts for water splitting and Zn–air batteries, *Adv. Mater.* 2(24), 7932 (2021)
118. D. S. Hall, D. J. Lockwood, C. Bock, and B. R. MacDougall, Nickel hydroxides and related materials: A review of their structures, synthesis and properties, *Proc. Math. Phys. Eng. Sci.* 471, 20140792 (2015)
119. T. Wang, J. Wu, Y. Liu, X. Cui, P. Ding, J. Deng, C. Zha, E. Coy, and Y. Li, Scalable preparation and stabilization of atomic-thick CoNi layered double hydroxide nanosheets for bifunctional oxygen electrocatalysis and rechargeable zinc–air batteries, *Energy Storage Mater.* 16, 24 (2019)
120. D. Wu, X. Hu, Z. Yang, T. Yang, J. Wen, G. Lu, Q. Zhao, Z. Li, X. Jiang, and C. Xu, NiFe LDH anchoring on Fe/N-doped carbon nanofibers as a bifunctional electrocatalyst for rechargeable zinc–air batteries, *Ind. Eng. Chem. Res.* 61(22), 7523 (2022)
121. D. Zhou, Z. Cai, Y. Jia, X. Xiong, Q. Xie, S. Wang, Y. Zhang, W. Liu, H. Duan, and X. Sun, Activating basal plane in NiFe layered double hydroxide by Mn^{2+} doping for efficient and durable oxygen evolution reaction, *Nanoscale Horiz.* 3(5), 532 (2018)
122. J. Ge, J. Y. Zheng, J. Zhang, S. Jiang, L. Zhang, H. Wan, L. Wang, W. Ma, Z. Zhou, and R. Ma, Controllable atomic defect engineering in layered $Ni_xFe_{1-x}(OH)_2$ nanosheets for electrochemical overall water splitting, *J. Mater. Chem. A* 9(25), 14432 (2021)
123. N. Thakur, M. Kumar, D. Mandal, and T. C. Nagaiah, Nickel iron phosphide/phosphate as an oxygen bifunctional electrocatalyst for high-power-density rechargeable Zn–air batteries, *ACS Appl. Mater. Interfaces* 13(44), 52487 (2021)
124. M. Zhang, J. Zhang, S. Ran, L. Qiu, W. Sun, Y. Yu, J. Chen, and Z. Zhu, A robust bifunctional catalyst for rechargeable Zn–air batteries: Ultrathin NiFe-LDH nanowalls vertically anchored on soybean-derived Fe-N-C matrix, *Nano Res.* 14(4), 1175 (2021)
125. Q. Wang, L. Shang, R. Shi, X. Zhang, Y. Zhao, G. I. N. Waterhouse, L. Z. Wu, C. H. Tung, and T. Zhang, NiFe layered double hydroxide nanoparticles on Co, N-codoped carbon nanoframes as efficient bifunctional catalysts for rechargeable zinc–air batteries, *Adv. Energy Mater.* 7(21), 1700467 (2017)
126. Y. Lin, H. Wang, C. K. Peng, L. Bu, K. Tian, Y. Zhao, J. Zhao, Y. G. Lin, J. M. Lee, and L. Gao, Co-induced electronic optimization of hierarchical NiFe LDH for oxygen evolution, *Small* 16(38), 2002426 (2020)
127. W. Wang, Y. Liu, J. Li, J. Luo, L. Fu, and S. Chen, NiFe LDH nanodots anchored on 3D macro/mesoporous carbon as a high-performance ORR/OER bifunctional electrocatalyst, *J. Mater. Chem. A* 6(29), 14299 (2018)
128. X. Cai, T. Jiang, and M. Wu, Confined growth of NiFe LDH with hierarchical structures on copper nanowires for long-term stable rechargeable Zn–air batteries, *Appl. Surf. Sci.* 577, 151911 (2022)
129. C. X. Zhao, J. N. Liu, J. Wang, D. Ren, J. Yu, X. Chen, B. Q. Li, and Q. Zhang, A $\Delta E = 0.63$ V bifunctional oxygen electrocatalyst enables high-rate and long-cycling zinc–air batteries, *Adv. Mater.* 33(15), 2008606 (2021)
130. L. Wan, Z. Zhao, X. Chen, P. Liu, P. Wang, Z. Xu, Y. Lin, and B. Wang, Controlled synthesis of bifunctional $NiCo_2O_4$ @FeNi LDH core–shell nanoarray air electrodes for rechargeable zinc–air batteries, *ACS Sustain. Chem. & Eng.* 8(30), 11079 (2020)
131. E. Meza, R. E. Diaz, and C. W. Li, Solution-phase activation and functionalization of colloidal WS_2 nanosheets with ni single atoms, *ACS Nano* 14(2), 2238 (2020)
132. S. Tian and Q. Tang, Activating transition metal dichalcogenide monolayers as efficient electrocatalysts for the oxygen reduction reaction *via* single atom doping, *J. Mater. Chem. C* 9(18), 6040 (2021)
133. Z. Qin, Z. Wang, and J. Zhao, Computational screening of single-atom catalysts supported by VS_2 monolayers for electrocatalytic oxygen reduction/evolution reactions, *Nanoscale* 14(18), 6902 (2022)
134. Q. Qi, J. Hu, Y. Zhang, W. Li, B. Huang, and C. Zhang, Two-dimensional metal–organic framework-based electrocatalysts for oxygen evolution and oxygen reduction reactions, *Adv. Energy Sustain. Res.* 2(3), 2000067 (2021)
135. S. Zhao, Y. Wang, J. Dong, C. T. He, H. Yin, P. An, K. Zhao, X. Zhang, C. Gao, L. Zhang, J. Lv, J. Wang, J. Zhang, A. M. Khattak, N. A. Khan, Z. Wei, J. Zhang, S. Liu, H. Zhao, and Z. Tang, Ultrathin metal–organic framework nanosheets for electrocatalytic oxygen evolution, *Nat. Energy* 1(12), 16184 (2016)
136. J. Huang, Y. Li, R. K. Huang, C. T. He, L. Gong, Q. Hu, L. Wang, Y. T. Xu, X. Y. Tian, S. Y. Liu, Z. M. Ye, F. Wang, D. D. Zhou, W. X. Zhang, and J. P. Zhang, Electrochemical exfoliation of pillared-layer metal–organic framework to boost the oxygen evolution reaction, *Angew. Chem. Int. Ed.* 57(17), 4632 (2018)
137. H. Li, M. Zhang, W. Zhou, J. Duan, and W. Jin, Ultrathin 2D catalysts with N-coordinated single Co atom outside Co cluster for highly efficient Zn-air battery, *Chem. Eng. J.* 421, 129719 (2021)
138. H. Jing, P. Zhu, X. Zheng, Z. Zhang, D. Wang, and Y. Li, Theory-oriented screening and discovery of advanced energy transformation materials in electrocatalysis, *Adv. Powder Mater.* 1(1), 100013 (2022)
139. R. Wang, L. R. Parent, S. Gopalan, and Y. Zhong, Experimental and computational investigations on the SO_2 poisoning of $(La_{0.8}Sr_{0.2})_{0.95}MnO_3$ cathode materials, *Adv. Powder Mater.* 2(1), 100062 (2023)